# Stresses and displacements in layered rocks induced by inclined (cone) sheets

Mohsen Bazargan and Agust Gudmundsson

Department of Earth Sciences, Queen's Building, Royal Holloway University of London, Egham TW20 0EX, UK (rock.fractures@googlemail.com)

## Abstract

Currently, the sheet-intrusion paths and geometries, including the sheet opening/thickness as well as the depth to sheet tip, are commonly determined from geodetic surface data using elastic dislocation models. These models assume the volcanic zone/volcano to be an elastic half space of uniform mechanical properties. Field observations, however, show that volcanic zones/volcanoes are composed of numerous layers whose mechanical properties (primarily Young's modulus) vary widely. Here we provide new numerical models on the effects of a typical variation in Young's modulus in an active volcanic zone/central volcano on the internal and surface stresses and displacements induced by a sheet-intrusion whose tip is arrested at a depth below the surface of 100 m. The sheet has a dip dimension (height) of 2 km. Its opening (thickness) depends on the magmatic overpressure, sheet dimension and host-rock Young's modulus. For the values used here, sheet thickness would be in the range of 0.5-1.4 m, similar to commonly measured sheet thicknesses in the field. The only loading is internal magmatic overpressure in the sheet of 5 MPa. The modelled crustal segment/volcano consists of 5 layers, all with the same Poisson's ratio (0.25). Each of the 4 uppermost layers is 10 m thick. Layer 1 (the top or surface layer) has a Young's modulus of 3 GPa, layer 2 a modulus of 20 GPa, layer 3 a modulus of 30 GPa, and layer or unit 5 a modulus of 40 GPa. We vary the Young's modulus or stiffness of the fourth layer from 10 GPa to 0.01 GPa, while the dip of the sheet takes the following values: 30°, 45°, 60° (for an inclined sheet) and 90° (for a dike). The resulting displacement and stresses are highly asymmetric across the sheet tip (except for the dike), with the main surface stresses and displacements being above the dipping sheet and highest for the 30°-dipping sheet. For comparison, three elastic half-space models of the same sheet configuration and loading but uniform Young's modulus in each model (40GPa, 20GPa, and 10 GPa), all yield much higher surface stresses and displacements than any of the layered models. As the stiffness of layer 4 decreases the surface stresses gradually decrease while changes in vertical displacements are comparatively small but greater in horizontal displacements. In particular, as the stiffness of layer 4 decreases from 10 GPa to 0.01 GPa, for the 30°-dipping sheet the maximum surface shear stress decreases from about 6.6 MPa to 2.2 MPa and the maximum tensile stress from about 6.9 MPa to about 2.3 MPa. Thus, even a single comparatively thin (10 m) soft layer close to the surface of a central volcano/volcanic zone (where such layers are almost universal), may cause a great change in the maximum sheet-induced stresses at the surface and, thereby, in any sheet-induced fracture pattern. Furthermore, the stress peaks do not coincide with the displacement peaks; fracture formation is most likely at the location of the stress peaks. The results have important implications for the correct interpretation of geodetic data and fracturing during unrest periods with magma-chamber rupture and sheet injection.

**Keywords:** volcano deformation, volcano stresses, crustal displacements, volcano unrest, geodetic data, numerical modelling

## 1. Introduction

One of the basic aims of volcanology is to understand the processes that happen inside a volcano during unrest periods. Some unrest periods do not result in magma-chamber rupture, but for those that do, forecasting the potential propagation path and geometry of the resulting sheet intrusion is of fundamental importance. This follows because most eruptions are supplied with magma through sheet intrusions; that is, are simply the consequence of a sheet intrusion, propagating as a magma-filled fracture, being able to make a path from its magma source to the surface (cf. Gudmundsson, 2020).

Sheet intrusions are of three main types: sills, dikes, and inclined (cone) sheets. Sills are concordant and thus close to horizontal in gently dipping or flat lava piles. Dikes are discordant and thus close to vertical in gently dipping or flat lava piles. Inclined sheets are, as the name implies, inclined; that is, neither vertical nor horizontal, and commonly with an average dip somewhere between 30° and 50° (e.g., Gudmundsson, 1995; Schirnick et al., 1999; Klausen, 2004; Ancochea et al., 2003, 2014; Burchardt and Gudmundsson, 2009) While the deformation induced by dikes and sills has been widely studied, that induced by inclined sheets has received much less attention. This is partly because there are very few reported cases where the geodetic (GPS and/or InSAR) surface-deformation data suggest an inclined sheet as the deformation source rather than a vertical dike, a horizontal sill, or a magma chamber. Perhaps the best recent geodetic data suggesting the emplacement of inclined sheets are those obtained from the Fernandina Volcano, Galapagos Islands, during its 2009 eruption (Bagnardi et al., 2013) and from the Cotopaxi Volcano, Ecuador, prior to its 2015 eruptions (Morales Rivera et al., 2017). In both cases the inferred inclined sheets are gently dipping (25°-34°) but while the sheet emplacement in Fernandina supplied magma to an eruption, the one in Cotopaxi did not - the sheet became arrested (the eruptions were fed by different types of intrusions).

The number of geodetically detected inclined sheets emplaced during unrest period in volcanoes is likely to increase much in the coming years and decades. This follows not only because of continuous improvements the quality of geodetic data and the associated modelling techniques, but because inclined sheets are much more common in many fossil (inactive) and active central volcanoes (stratovolcanoes, basaltic edifices; polygenetic volcanoes) than either sills or dikes (Fig. 1). In fact, close to fossil shallow magma chambers, that is, plutons, inclined sheets may constitute 70-80% of the rock (Fig. 2). Inclined sheets are best studied in three dimensions in deeply eroded volcanic edifices (Figs. 2-4; Bell et al., 1994; Geldmacher et al., 1998; Schirmick et al., 1999; Ancochea et al., 2003, 2014; Burchardt and Gudmundsson, 2009; Troll and Carracedo, 2016). But many inclined sheets can be observed in active volcanoes, even if as yet not detected geodetically. For example, some of the fissures associated with the Askja Central Volcano in Iceland are clear examples of inclined sheets (Gudmundsson, 1998). Many flank eruptions in major volcanic edifices are likely to be fed by inclined sheets or radial dikes (Fig. 1).

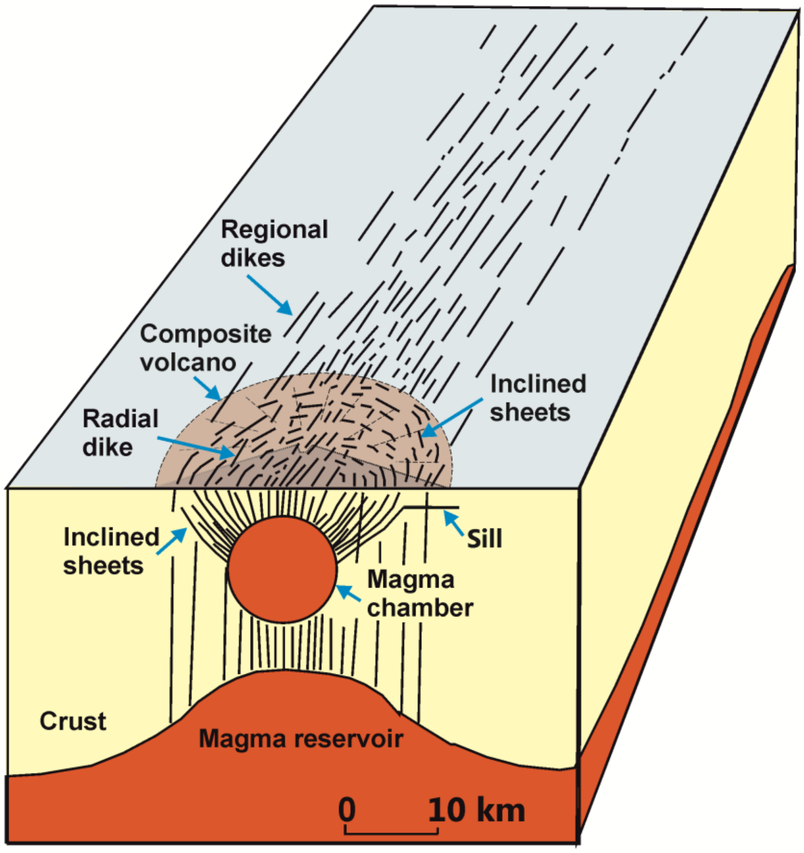


*Fig. 1 Internal structure of a typical rift-zone volcanic system fed by a deep-seated reservoir as well as a shallow magma chamber which supplies magma to the central (here composite) volcano. The composite volcano is mainly supplied with magma from thin inclined sheets and radial dikes injected from the shallow chamber, whereas the eruptions outside the central volcano are primarily supplied with magma through much thicker regional dikes. Most dikes and inclined sheets do not reach the surface to erupt but stop, become arrested, at contacts between dissimilar layers at some depth – some deflecting into sills at these contacts. The local swarm that forms above the shallow chamber is what is referred to as a sheet swarm, whereas the swarm outside the volcano is the regional dike swarm.*

When assessing the processes inside a volcano during an unrest period with magma-chamber rupture and sheet injection, it is important to be able to distinguish between the types of sheet-intrusions. Clearly, the displacements and stresses induced by a vertical dike are very different from those induced by a horizontal sill (e.g., Dzurisin, 2006; Bagnardi et al.., 2013; Barnett and Gudmundsson, 2014; Morales Rivera et al, 2017). But the displacements and stresses induced by an inclined sheet are somewhere between those induced by dikes and sills. In order to forecast likely propagation paths and eventual eruptions, we must be able to distinguish the displacements and stresses due to an inclined sheet from those of either a dike or a sill.

The present paper focuses on the stresses and displacements induced by inclined sheets. The emphasis is on new numerical models as to the effects of mechanical layering in volcanoes and crustal segments on internal and surface stresses and displacements. For comparison, we show stresses and displacements inferred for inclined sheets in elastic half-space (non-layered) models (of uniform Young’s modulus). We also provide a general overview of inclined sheets, using detailed studies of sheets in Iceland and Scotland as a basis.

## 2. Field observations

Inclined sheets were first described in connection with studies of the Tertiary volcanoes of Scotland (Harker 1904), such as on the island of Skye and the peninsula of Ardnamurchan.

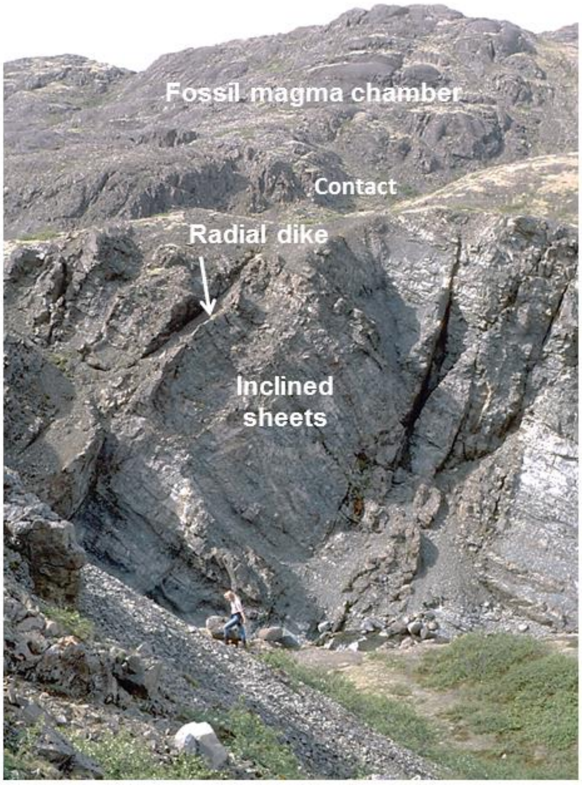


*Fig. 2. Dense swarm of inclined sheets in the gully of Geitafellsgil in the fossil central volcano Geitafell in Southeast Iceland (located in Fig. 3 of Burchardt and Gudmundsson, 2009). When the chamber was active (the fossil chamber is now a gabbro pluton) its roof was at about 2 km below the surface of the associated central volcano. Part of the local swarm of inclined sheets and radial dikes is seen here. The sheets constitute 80-100% of the rock close to the fossil magma chamber. Also indicated is the main contact between the chamber and the sheet swarm. The person provides a scale.*

These were later referred to as cone sheets apparently on the assumption that the excess pressure in the source chamber would generate conical fractures into which the magma would flow. On this view the sheets would be parts of cones, meeting at a focal point, which was supposed to be at the source. The sheets would then be concentric and inward-dipping at an average angle of about 45º and all intersect at a certain point, the apex or summit of the chamber.

In the past decades, cone sheets have been studied in many eroded volcanoes. The results indicate that they do not, as a rule, form conical fractures, and their attitudes vary much, with many cross-cutting sheets (e.g., Gautneb et al., 1989; Gautneb and Gudmundsson, 1992;

Gudmundsson, 1995, 1998; Klausen, 2004, 2006; Pasquare and Tibaldi, 2007; Burchardt and Gudmundsson, 2009; Siler and Karson, 2009; Tibaldi et al., 2011, 2013; Bistacchi et al., 2012). The term cone sheet is thus regarded as less appropriate than the general term inclined sheet, which is now more commonly used. The main reasons for using the term inclined sheets is that the structures are sheet-like, and their dips are mostly much shallower than those of dikes, while being much steeper than those of sills.

*2.1 Mechanical characteristics*

The mechanical characteristics of geological structures such as sheet-intrusions can, of course, only be determined accurately by field observations. This applies to their typical attitude (strike and dip), thickness, under what conditions they become arrested and, in

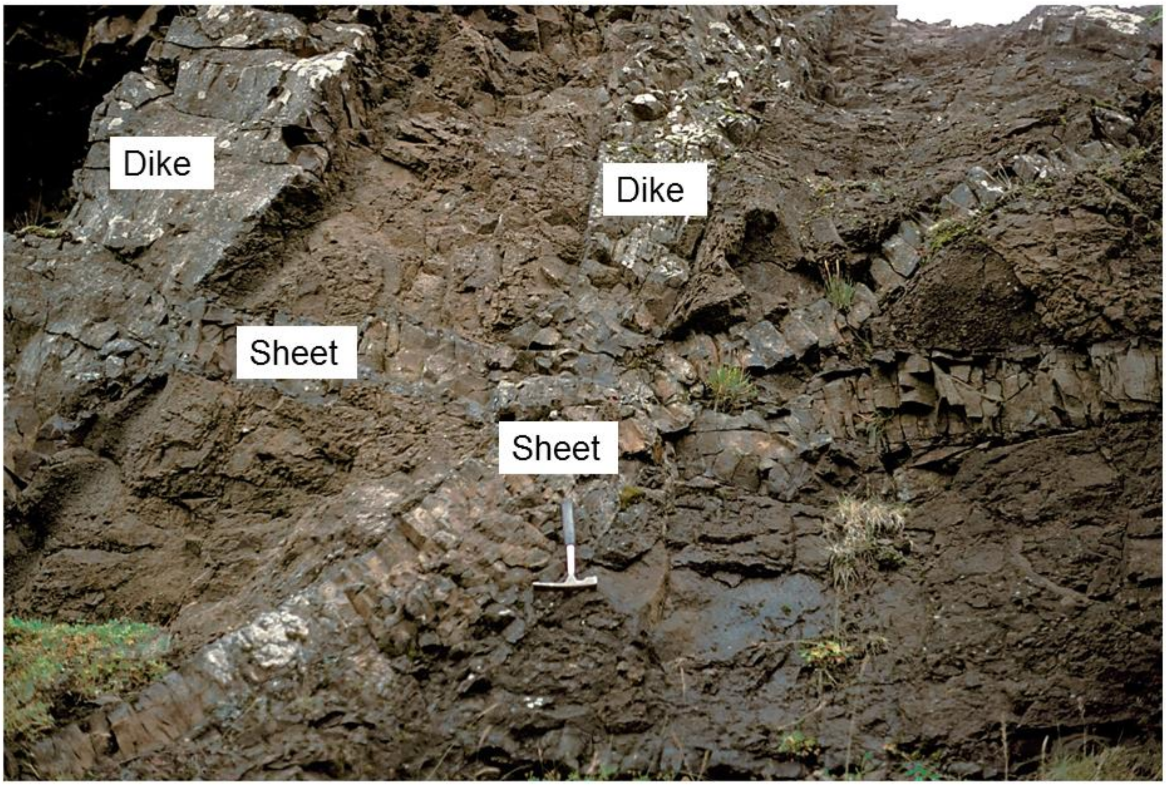


*Fig. 3. Cross-cutting inclined sheets and basaltic dikes in lake sediments in the canyon of the river Laxa in South Iceland. The length of the hammer is about 30 cm. The cross-cutting relationship here and in thousands of other outcrops show that the great majority of inclined sheets and dikes are extension fractures (cf. Figs. 2 and 4).*

particular, the type of fracture they are. Below we present some general results on the attitude and thickness of sheets, using primarily data from well-studied sheet swarms in Iceland. We also discuss the way that sheets are seen arrested in the field. To model sheets, however, we need to know what types of fractures they are; in particular, whether they shear fractures (faults) or extension fractures. Field studies of thousands of cross-cutting relationships between inclined sheets and the host-rock layers, particularly lava flows (and sills) and pyroclastic layers, as well as among inclined sheets and between sheets and dikes provide clear evidence that the great majority of inclined sheets are extension fractures (Figs. 3 and 4). It follows that they can be modelled as mode I cracks, as is discussed below.

This is a very important conclusion, with wide implications for modelling and forecasting sheet-propagation paths and sheet-fed eruptions. It is therefore worthwhile to clarify this point. No modelling - analogue, analytical, numerical - can determine what mechanical type a rock fracture is: only direct observations of the fracture in the field and on images make such a decision possible. Decades ago it was unclear what mechanical types of fracture inclined sheets are – they were assumed to be extension fractures in the first mechanical models provide to explain them (Anderson, 1936) - and several authors (e.g., Phillips, 1974) speculated that they might occupy shear fractures, that is, faults. This was plausible at the time, since extensive datasets on cross-cutting relations did not exist. In the past decades, many thousand cross-cutting relationships have been observed, however, showing that the great majority of inclined sheets are extension fractures (e.g., Gautneb et al., 1989; Gautneb


*Fig. 4. Dense sheet swarm in the gully of Efstafellsgil in the fossil central volcano Geitafell in Southeast Iceland (located in Fig. 3 of Burchardt and Gudmundsson, 2009). The sheets show numerous cross-cutting relationships (some indicated by the letter C) among inclined sheets. The average thickness of the sheets seen here is about 0.6 m.*

and Gudmundsson, 1992; Gudmundsson, 1995, 1998; Klausen, 2004, 2006; Pasquare and Tibaldi, 2007; Burchardt and Gudmundsson, 2009; Siler and Karson, 2009; Tibaldi et al., 2011, 2013; Bistacchi et al., 2012). The same applies to other sheet-like intrusions, such as dikes (e.g., Gudmundsson, 1995, 1998; Geshi et al., 2010; Galindo and Gudmundsson, 2012; Drymoni et al., 2020).

Dikes and inclined sheets may, however, occasionally follow shear fractures, mostly existing faults, along parts of their paths (e.g. Dering et al., 2019; Drymoni et al., 2020; Gudmundsson, 2020). This can happen under certain restricted conditions, all of which can be formulated and explained in terms of energy considerations (Gudmundsson, 2020). These conditions, which would mainly be satisfied by steeply dipping normal faults, are rarely met and do not change the field results that the great majority of inclined sheets (and dikes and sills) are extension fractures and should be modelled as mode I cracks. The field results can easily be checked in in any of the numerous well-exposed sheet and dike swarms worldwide. Despite these clear field results, however, there are still papers being published where it is assumed that inclined sheets are primarily shear fractures (e.g., Gerbault et al., 2012; Galland et al., 2014; Guldstrand et al., 2017; Stephens et al., 2018). Since inclined sheets are magma-driven fractures, rock rupture or failure occurs under high fluid pressure. These authors would thus have to explain how shear failure at the contact with a fluid body can be reached before tensile failure. Given that the tensile strength of rocks is about half the shear strength – as follows from the Modified Griffith criterion and is confirmed by measurements (e.g. Gudmundsson 2011a, 2020) - it is unclear how shear failure before tensile failure could

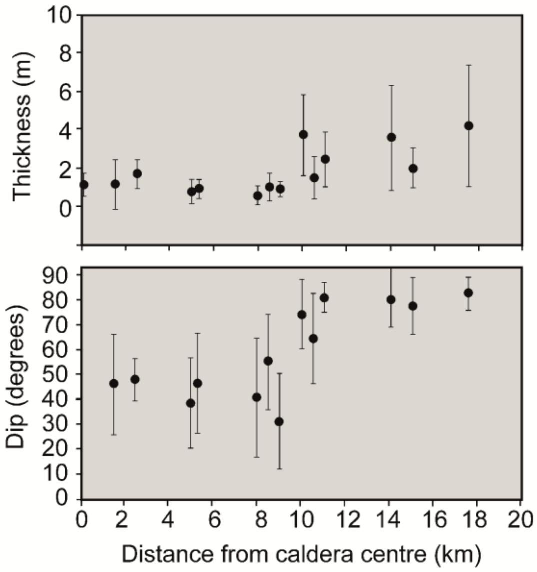


*Fig. 5. Abrupt increase in thickness and dip of inclined sheet at a distance of about 9 km from the centre of the caldera, located above the fossil shallow magma chamber of the central volcano of Reykjadalur in West Iceland (located and described in Gautneb and Gudmundsson, 1992). At this distance there is a change from a local sheet swarm to a regional dike swarm. Vertical error bars indicate the range in values at each measurement station.*

happen at the contact with a fluid body. That the field results contradict the idea that inclined/cone sheets initiate as shear fractures is recognised by some of these authors who propose that 'magma injection, deformation of the host rocks, and opening of the propagating cone sheet fracture could obliterate any signs of initial shear failure, in nature.' (Galland et al., 2014). That proposal makes the idea of inclined/cone sheets being shear fractures untestable in principle by any actual field data.

Based on the field observations and theoretical considerations discussed above (and by Gudmundsson, 2020), in this paper we will model inclined sheets as extension fractures. More specifically, we model them as fluid-driven fractures (hydrofractures) where the appropriate fracture-mechanics model is that of a mode I crack. As indicated below, this modelling implies that the propagation paths of the inclined sheets follow the trajectories of the maximum compressive principal stress, $\sigma_1$ (and are thus perpendicular to the minimum compressive (maximum tensile) principal stress, $\sigma_3$). This conclusion as to the stress-controlled propagation paths of inclined sheets is well established for fluid-driven fractures in general, including dikes (Anderson, 1936; Valko and Economides, 1995; Meriaux and Lister, 2002; Gudmundsson, 2020) and forms the basis of hydraulic fracturing stress measurements in drill holes (Amadei and Stephansson, 1997; Gudmundsson, 2011a).

## 2.2 Field characteristics

The main characteristics of inclined sheets, primarily based on data from Iceland and Scotland (Gautneb et al., 1989; Gautneb and Gudmundsson, 1992; Bell et al., 1994; Gudmundsson, 1995, 1998; Geldmacher et al., 1998; Klausen, 2004, 2006; Pasquare and Tibaldi, 2007; Siler and Karson, 2009; Tibaldi et al., 2011, 2013; Bistacchi et al., 2012), as well as data from the Canary Islands and other ocean islands (Schirnick et al., 1999; Ancochea et al., 2003, 2014; Troll and Carracedo, 2016), may be summarised as follows:

- The sheets occur in swarms that are mostly confined to central volcanoes, that is, stratovolcanoes, basaltic edifices, and calderas. A typical swarm may contain many

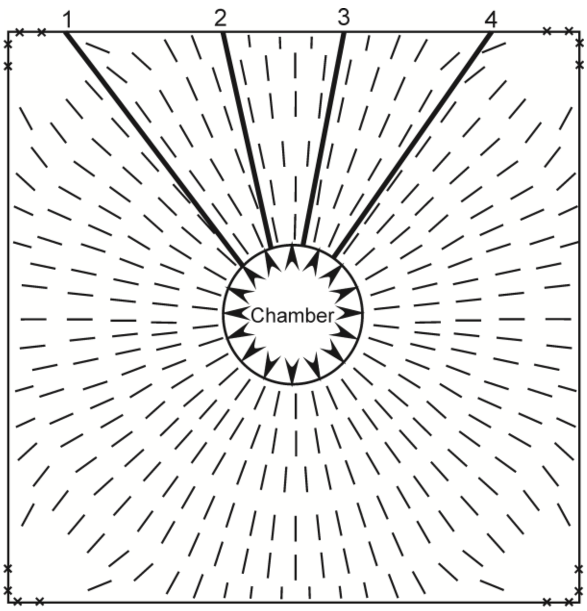


*Fig. 6. Inclined sheet paths follow the $\sigma_1$- trajectories, as indicated here for four sheets (marked 1-4), injected from a shallow magma chamber of a circular vertical cross-section. In this numerical model the crustal segment is homogeneous and isotropic and the only loading is internal chamber excess magmatic pressure $p_e$ of 10 MPa. So long as the magma has any significant overpressure (Eq. 3) all sheets should reach the surface.*

- thousand sheets (Figs. 2 and 4), the swarm being circular or slightly elliptical in plan view, and commonly many kilometres in radius. In Iceland, the largest swarm is about 18 km in diameter. In the Canary Islands, the sheet swarm of La Gomera is about 10 km in diameter (Ancochea et al., 2003) and that of Gran Canaria about 20 km in diameter (Schirnick et al., 1999). Similarly, the sheet swarm of the island of Boa Vista, one of the Cape Verde Islands, is about 22 km in diameter (Ancochea et al., 2014).
- In some sheet swarms, the dip changes with distance from the centre of the swarm (centre of the central volcano to which the swarm belongs). For example, in the Reykjadalur Volcano in West Iceland, there is an abrupt increase in dip and thickness of sheet-like intrusions at 9 km from the centre, that is, at the margin of the swarm. Thus, at that distance the regional dike swarm take over from the local sheet swarm (Fig. 5; Gautneb and Gudmundsson, 1992). In many swarms, however, there is a gradual decrease in sheet dip towards the margins of the swarm. For example, in the swarm of Boa Vista the mean dip of sheets is about 40° in the central part but decreases to about 30° in the marginal parts (Ancochea et al., 2014). Similarly, the mean dip of sheets in the central part of the swarm of La Gomera is about 65°, but decreases to about 40° in the marginal parts (Ancochea et al., 2003). By contrast, the

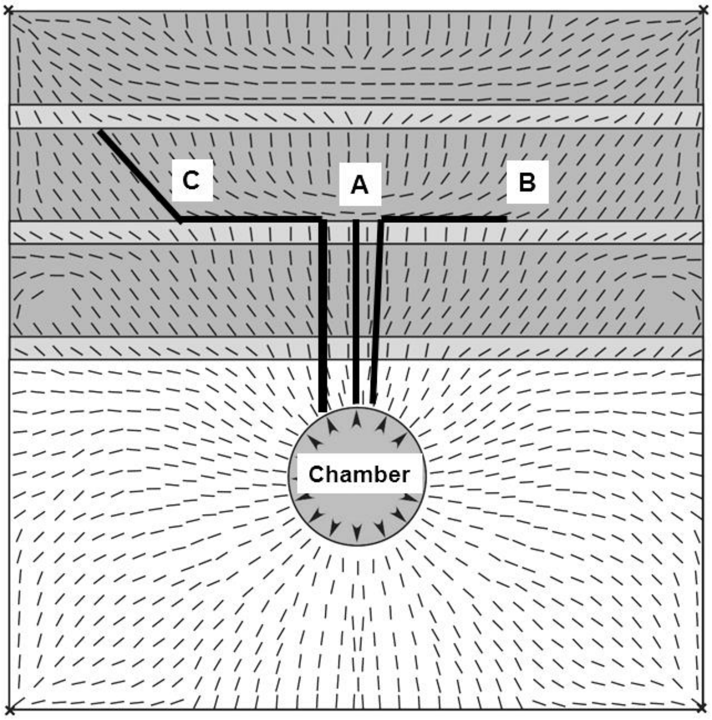


*Fig. 7. Potential paths (parallel to the indicated $\sigma_1$ trajectories) of sheets (dikes, sills, and inclined sheets) injected from a shallow magma chamber of a circular cross-section subject to 5 MPa internal excess pressure as the only loading. The thin layers are compliant (soft, 1 GPa) whereas the thick layers stiff (100 GPa). Sheet path A becomes arrested at the contact where the $\sigma_1$- trajectories flip 90º while path B changes into a sill. At the contact, path C first changes into a sill and then into an inclined sheet.*

- average dip of sheets at a given elevation remains the same in the centre and in the marginal parts of the swarm of Gran Canaria – about 35° - but the dip increases somewhat with elevation (Schirnick et al., 1999). The intensity of the swarm – number of sheets per unit length of traverse – as well as the average sheet thickness decrease markedly with elevation in some swarms (Klausen, 2004).
- In deeply eroded central volcanoes, the sheets can commonly be traced into the source shallow magma chamber (Fig. 2). The fossil magma chamber is currently exposed as a pluton, most commonly a mafic body (a gabbro body in Fig. 2). There is then no doubt about the source of the inclined sheets. Suggestions that the sheets originate somehow from dikes, particularly the tops of dikes (Galland et al., 2014), are not supported by any field data that we are aware of. In particular, such ideas are in contradiction with the facts that in the swarms (1) sheets are many times more frequent than dikes and also (2) commonly more evolved chemically (Gautneb et al., 1989; Gautneb and Gudmundsson, 1992). Furthermore, (3) hundreds of arrested dike tips (dike tops) have been observed and these are not seen to change into inclined sheets (Gudmundsson, 2003, 2020; Geshi et al., 2010; Galindo and Gudmundsson, 2012; Al Shehri and Gudmundsson, 2018; Bazargan and Gudmundsson, 2019; Drymoni et al., 2020).
- The sheets commonly make up 60-100% of the rock in short traverses close to their sources, that is, close to the margins of the associated plutons that constitute the

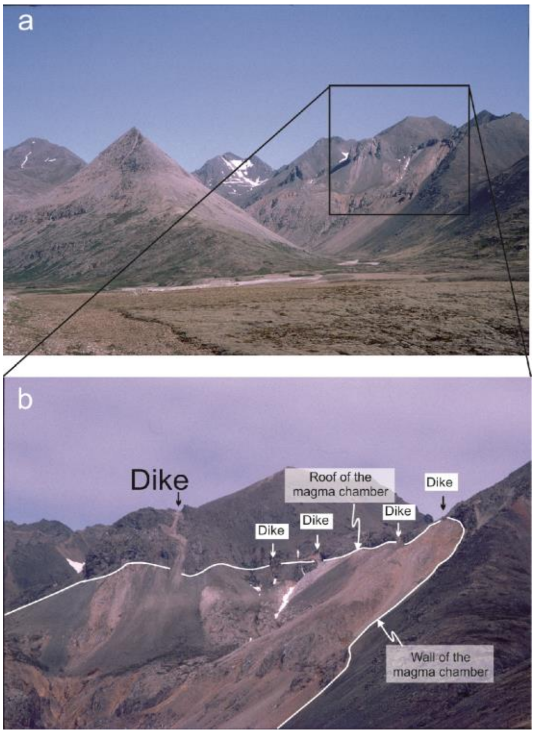


*Fig. 8. Part of the roof and the walls of a fossil shallow magma chamber of Slaufrudalur in Southeast Iceland (located and described in Gudmundsson, 2020). Many sheets, primarily dikes, cut the roof. The granophyre pluton is hosted by a pile of basaltic lava flows. When it was active its roof was about 1.5 km below the surface of the associated volcanic zone. Many dikes cut the roof. The thick one to the left on the figure changes its path from vertical to inclined and then again to vertical.*

- frozen magma chambers (Fig. 2). The percentage, however, declines rapidly with distance from the fossil source magma chamber (e.g., Klausen, 2004) and may be as low as 6-8% in kilometre-long traverses.
- The attitude (strike and dip) of the sheets within a swarm varies widely. Some swarms show two peaks in the sheet dip distribution: steep-dipping sheets dip at 75°-90º whereas shallow-dipping sheets dip at 20°-50º. As indicated above, the steep-dipping sheets are mostly confined to the central part of the swarm (e.g., Ancocea et al., 2003, 2014), where many of them could be classified as radial dikes (Fig. 1). The shallow-dipping sheets are mostly confined to the marginal parts of the swarm, where some of them could be classified as sills (Fig. 1). The average dip in several swarms in Iceland

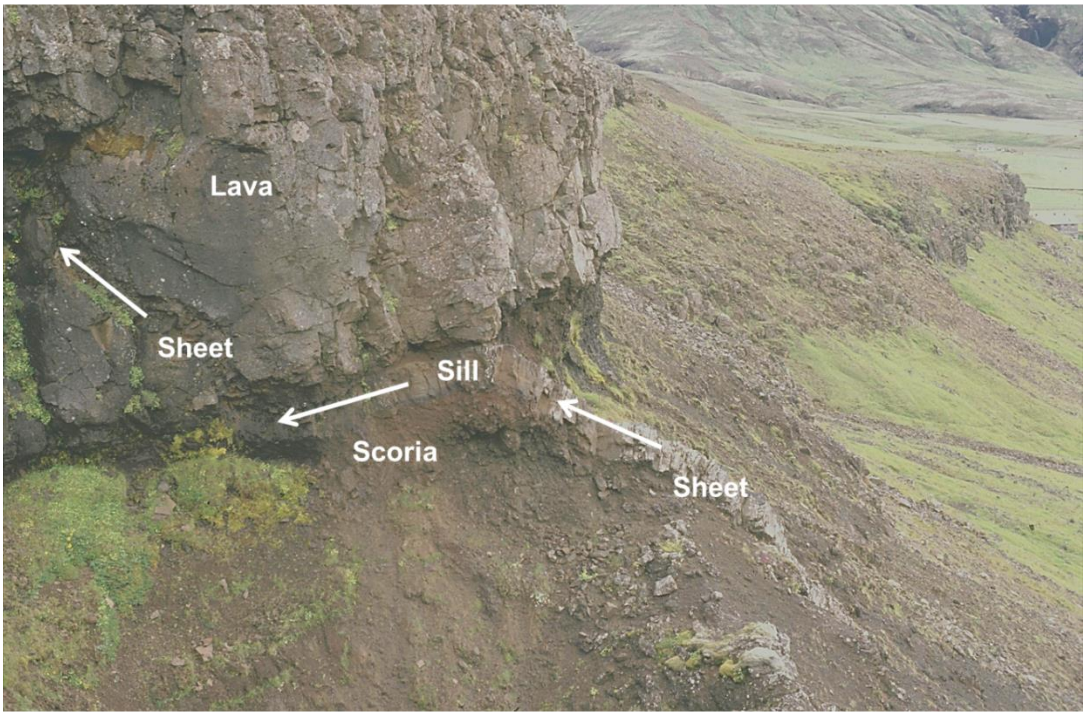


*Fig. 9. Propagation path of a basaltic inclined sheet, 0.5-1 m thick, in Southwest Iceland. The sheet deflects along a contact between a stiff basaltic lava flow and a compliant or soft scoria layer and then follows an inclined path through the lava flow.*

- is about 34° (Gudmundsson et al., 2018), very similar to that of the swarms of Boa Vista (Ancochea et al., 2014) and Gran Canaria (Schirnick et al., 1999) discussed above.
- The sheets range in thickness form a few centimetres to about ten metres, and occasionally more. The thickness of most basaltic sheets, however, is between 0.1 and 1 m (e.g., Gudmundsson, 1995; Geldmacher et al., 1998; Klausen, 2004). The more evolved sheets tend to be thicker, with average values in swarms occasionally of 2-4 m (Schirnick et al., 1999).
- Like the regional dikes, the sheets are commonly segmented and offset, some of the offset parts being connected by thinner segments, or igneous veins. Individual segments tend to be flat ellipses, both in plan views as well as in vertical sections. But many show irregularities in geometries and abrupt changes in propagation paths.

- While the great majority of the sheets are mafic (and intermediate at convergent boundaries), the sheets are, on average, somewhat more evolved in composition than the regional mafic dikes (Gautneb et al., 1989; Gautneb et al., 1992; Troll and Carracedo, 2016). This is understandable since the sheets are confined to shallow crustal magma chambers where crystal fractionation and anatexis are common (e.g., Bell et al., 1994; Geldmacher et al., 1998) whereas many of the regional dikes derive from deep-seated magma reservoirs hosting primitive melts. In addition to the mafic sheets, intermediate, felsic and composite sheets are common in many swarms (Gautneb et al., 1989; Bell et al., 1994; Geldmacher et al., 1998; Schirnick et al.,

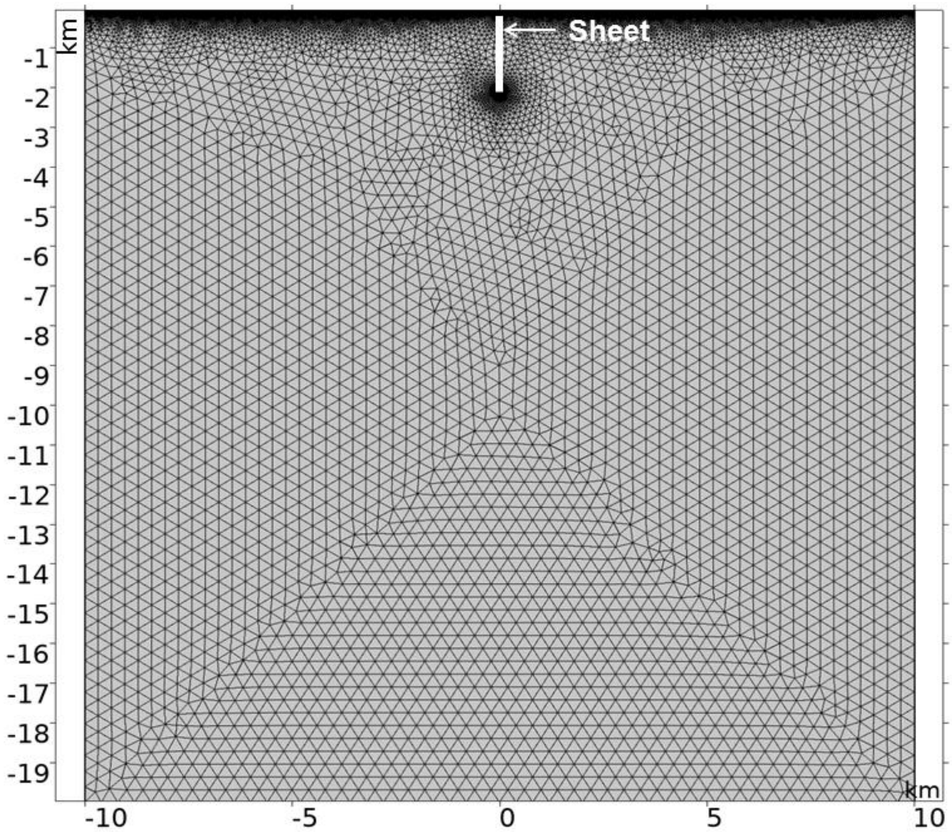


*Fig. 10. Setup of the Comsol model with the 2 km tall sheet (dip dimension) and 2 m thick in the central upper part (indicates as thick white line) of the model (whose dimensions are 20 km × 20 km). The complete mesh consists of 46,945 domain elements and 7434 boundary elements. The minimum element quality is 0.3985 m.*

1999; Ancochea et al., 2003, 2014; Troll and Carracedo, 2016). These are generally thicker, on average, than the mafic sheets, as indicated above.

A comparison with the regional dikes suggests the following main differences. Inclined sheets are generally (1) shorter, (2) thinner, (3) more gently dipping, (4) of more evolved composition, and (5) with a much higher frequency (number per unit length of profile) than regional dikes. All these differences relate to most or all of the inclined sheets being derived from shallow crustal magma chambers whereas many of the regional dikes derive from deeper reservoirs with a more primitive magma. There are, of course, many dikes that are injected from the shallow magma chambers. These include, in particular, radial dikes (Fig. 1). However, these, as well as dikes within the swarms of inclined sheets, are commonly regarded as parts of the local sheet swarms rather than parts of the regional dike swarms. This follows because the dikes of the sheet swarms are controlled as regards composition, attitude, and thickness by the local stress fields of the shallow magma chambers, rather than the regional stress fields that control the formation of the regional dikes.

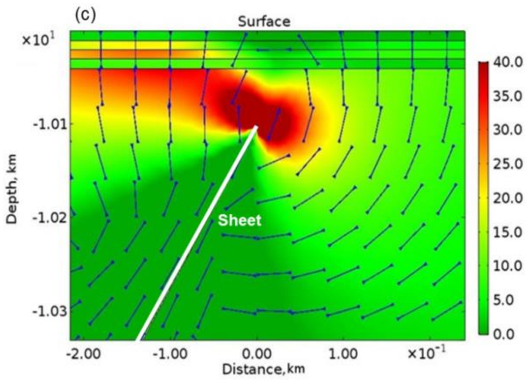


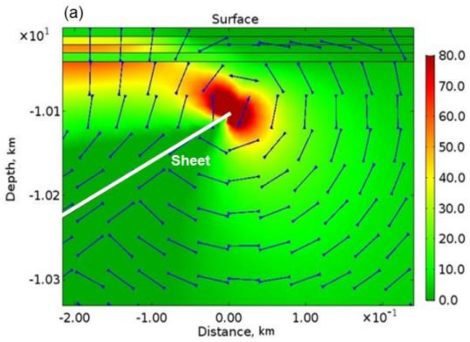


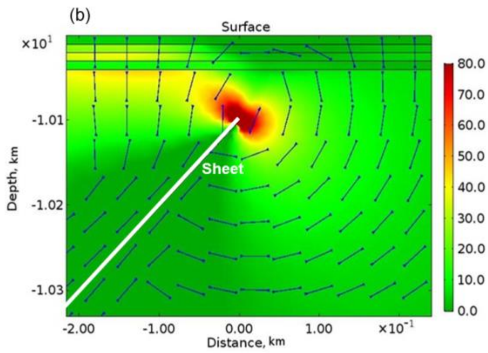


*Fig. 11. The maximum principal tensile stress ($\sigma_3$) inside the model in mega-pascals (vertical colour scale to the right of the model shows the magnitude in MPa). Layer 4 has a stiffness of 10 GPa. (a) Sheet dipping 30°. (b) Sheet dipping 45°. (c) Sheet dipping 60°.*

## 3. Mechanics of emplacement

Before we come to the numerical results on the sheets and the stresses and displacements that they induce, we first discuss briefly the conditions of shallow magma-chamber rupture and sheet injection followed by the mechanics of sheet emplacement.

### 3.1 *Magma-chamber rupture*

The three main processes that may result in magma-chamber rupture and sheet injection are:

- Magma is added to the chamber, usually from a deeper source reservoir below (Fig. 1) As the volume of magma in the chamber increases, local tensile stress at the boundary of the chamber – in the chamber roof - gradually reaches roughly the tensile strength of the host rock. Depending on the local stress field (Figs. 6 and 7), the resulting magma-filled fracture that is injected from the chamber is either a dike or an inclined sheet (or, rarely, a sill).
- Gradual extension of the crustal segment hosting the chamber, such as in continental rift zones or at divergent plate boundaries in general, results in the concentration of tensile stress at the boundary which, eventually, reaches the tensile strength of the host rock. Again, depending on the local stress field (Figs. 6 and 7), a dike or an inclined sheet (occasionally, a sill) is injected.
- Magma addition and extension commonly operate together, particularly at divergent plate boundaries.

The condition for rupture and sheet injection is given by (Gudmundsson, 2011a,b):

$$p_l + p_e = \sigma_3 + T_0 \qquad (1)$$

where $p_l$ denotes the lithostatic stress at the rupture site at the boundary of the magma chamber (normally the roof or the walls; rarely the floor), $p_e$ is the excess magmatic pressure in the chamber (the pressure in excess of $\sigma_3$, the minimum compressive or maximum tensile principal stress), and $T_0$ the in situ tensile strength at the rupture site. Eq. (1) can also be written on the form:

$$p_t = \sigma_3 + T_0 \qquad (2)$$

where $p_t = p_l + p_e$ is the total fluid pressure in the chamber at the time of rupture. Eqs. (1) and (2) imply that when the total fluid pressure in the chamber reaches the combined value of the minimum principal compressive (maximum tensile) stress and the in-situ tensile strength, the chamber (roof) ruptures and injects a magma-filled fracture. Depending on the local stress trajectories, this fracture may either be a vertical dike or an inclined sheet (Figs. 6 and 7).

(a)

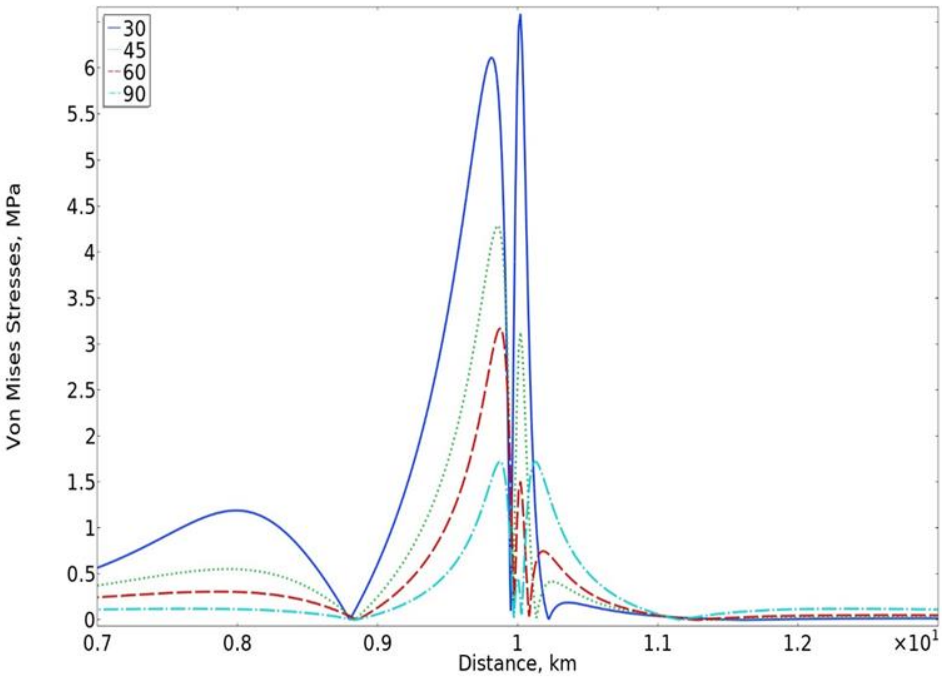
30
45
60
90
Von Mises Stresses, MPa
0
0.5
1
1.5
2
2.5
3
3.5
4
4.5
5
5.5
6
0.7
0.8
0.9
1
1.1
1.2
×10¹
Distance, km

(b)

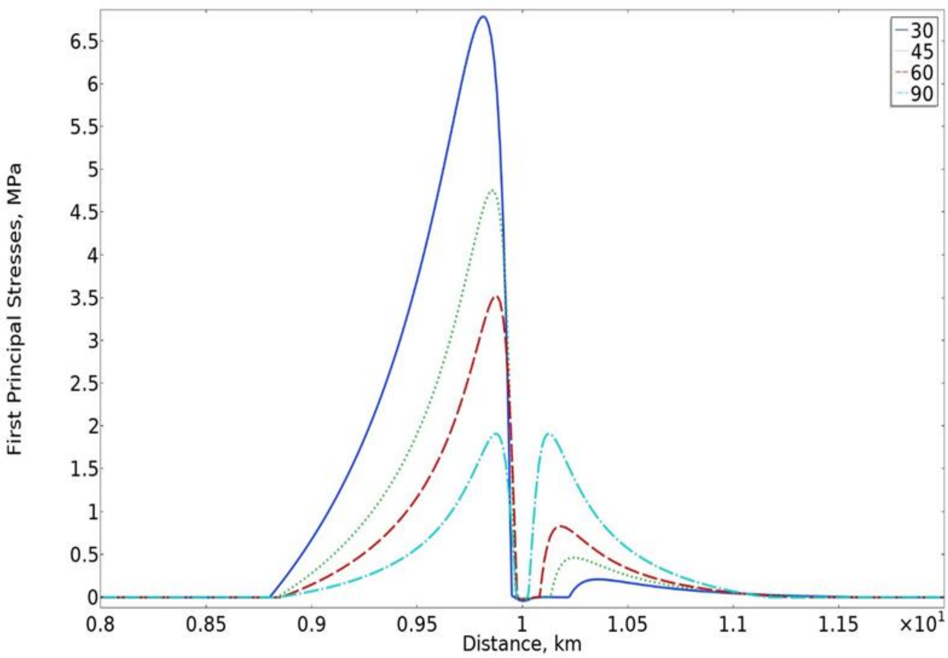
30
45
60
90
First Principal Stresses, MPa
0
0.5
1
1.5
2
2.5
3
3.5
4
4.5
5
5.5
6
6.5
0.8
0.85
0.9
0.95
1
1.05
1.1
1.15
×10¹
Distance, km

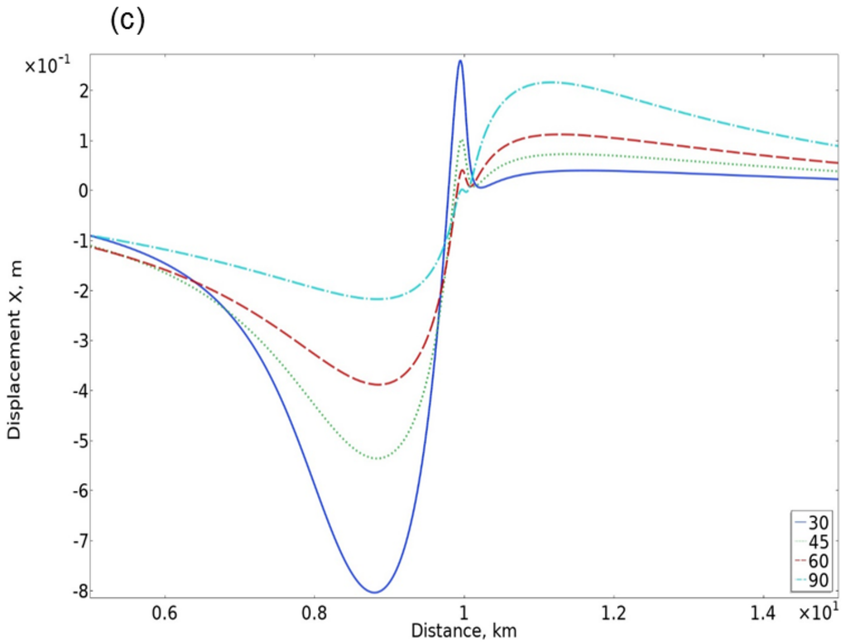


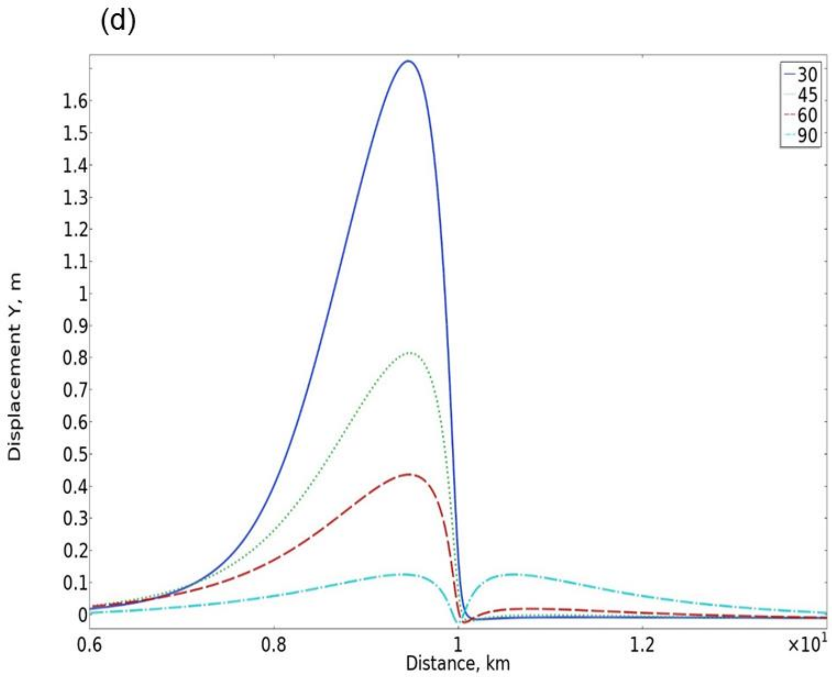


*Fig. 12. Surface stresses and displacements induced by an inclined sheet with a dip dimension of 2 km and 5 MPa internal magmatic pressure as the only loading. Layer 4 has a stiffness of 10 GPa. (a) Von Mises shear stress. (b) Maximum principal tensile stress ($\sigma_3$). (c) Horizontal displacement. (d) Vertical displacement.*

It is important to realise that rupture and sheet/dike injection would always occur at some irregularities at the boundary of the chamber, where the local stress concentration is significantly higher than that around the magma chamber as a whole. Thus, it is the local stress concentration at an irregularity in the roof or the walls of the magma chamber (rarely

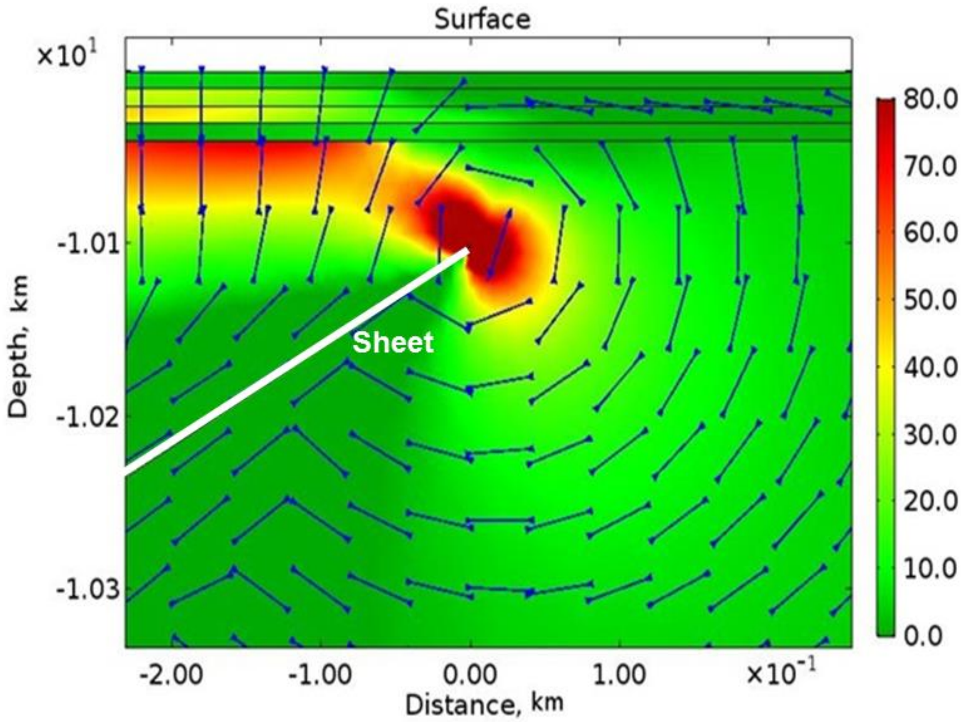


*Fig. 13. The maximum principal tensile stress ($\sigma_3$) inside the model in mega-pascals (vertical colour scale to the right of the model shows the magnitude in MPa) for a sheet dipping 30°. Layer 4 has a stiffness of 1 GPa.*

the floor of the chamber) that results in rupture rather than the concentration around the chamber as a whole of a given general geometric shape. It follows that Eqs. (1) and (2) are generally appropriate as conditions for rupture irrespective of the overall approximate shape of the chamber (oblate ellipsoid or sill-like, spherical, or prolate ellipsoid, for example).

3.*2 Sheets form their own fractures*

The sheet-fracture is an extension fracture, a hydrofracture, to which Eqs. (1) and (2) apply. This is in accordance with the field results, discussed above, which show clearly that the great majority of inclined sheets and dikes occupy extension fractures. Eqs. (1) and (2) also imply that it is the magma itself that breaks or ruptures the rock, in a manner analogous to artificial hydraulic fracturing used to increase the permeability in reservoirs of various types (Valko and Economides, 1995) and for in-situ stress measurements and tensile-strength measurements in drill holes (Amadei and Stephansson, 1997). This conclusion rests on direct field observations as well as theoretical considerations. There are no wide-open extension fractures at many kilometres depth waiting to be filled with magma, neither in rift zones nor anywhere else in the Earth's crust. Griffith's fracture theory explains why large tension fractures (formed by tensile forces/stresses and not by fluid pressure – the latter are hydrofractures) cannot form at greater depths than about 1 km, and do usually not extend from the surface to depths exceeding a few hundred metres (Gudmundsson, 2011a). Direct

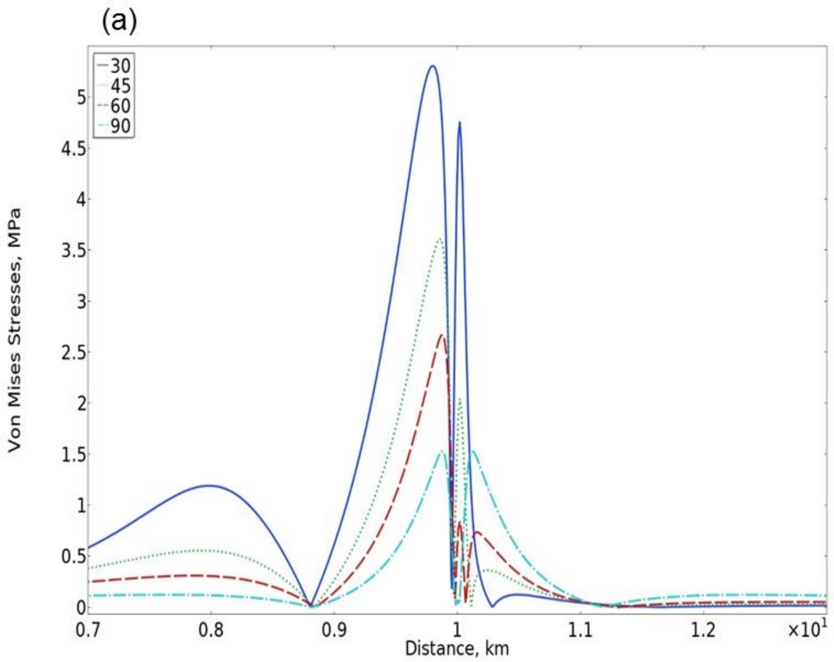


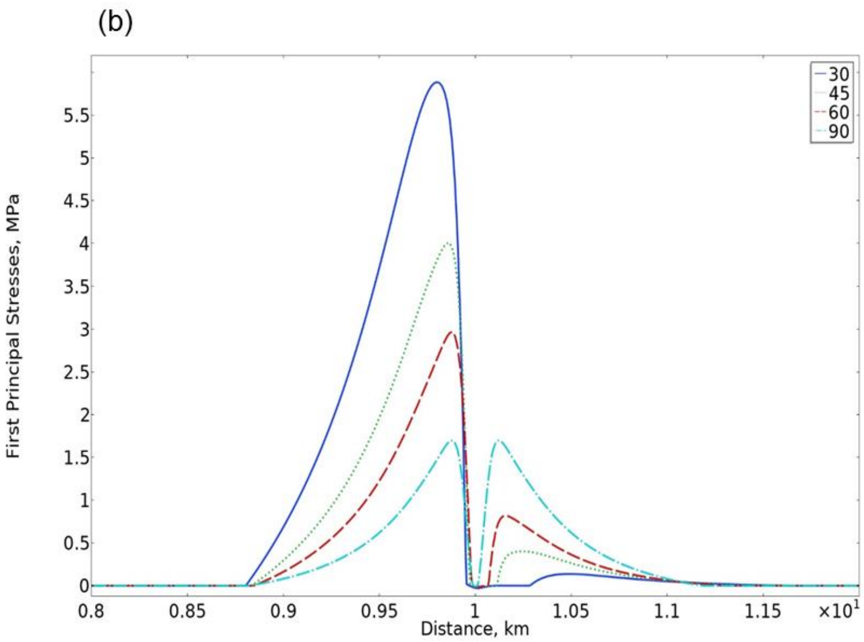

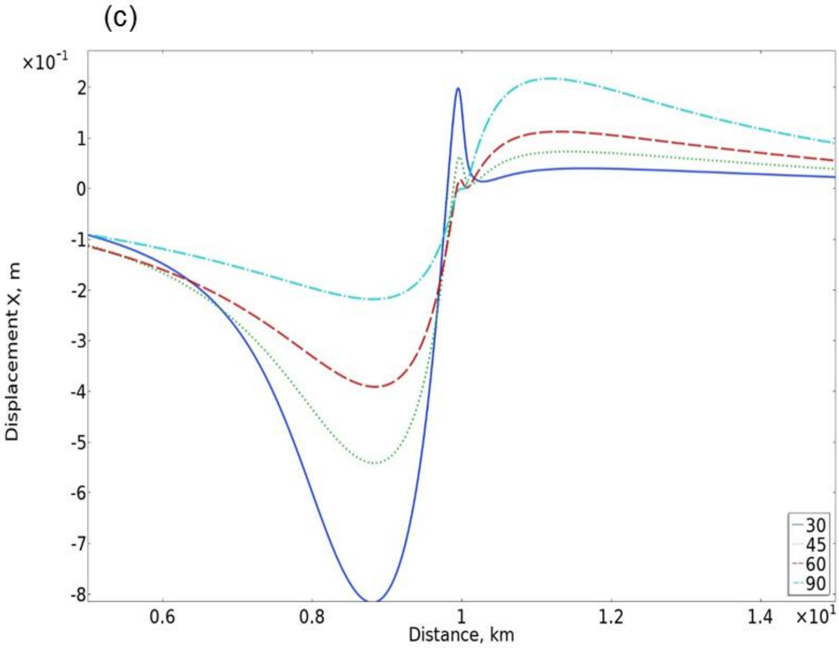


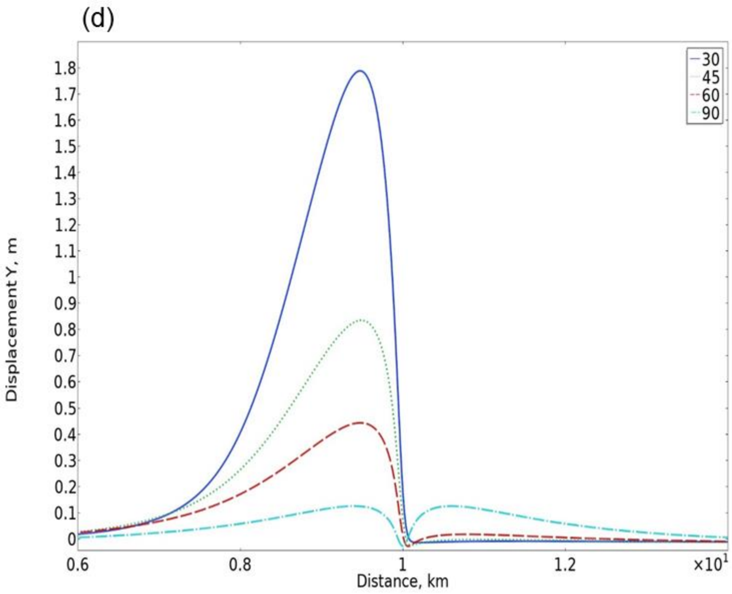


*Fig. 14. Surface stresses and displacements induced by an inclined sheet with a dip dimension of 2 km and 5 MPa internal magmatic pressure as the only loading. Layer 4 has a stiffness of 1 GPa. (a) Von Mises shear stress. (b) Maximum principal tensile stress ($\sigma_3$). (c) Horizontal displacement. (d) Vertical displacement.*

observations in caldera walls, erosional cliffs, and other sections into active and inactive volcanoes and rift zones show that large tension fractures only exist at very shallow depths. Furthermore, large inclined fractures, such as would be suitable paths for inclined sheets, would normally be shear fractures, faults, and, as mentioned, most inclined sheets do not occupy faults.

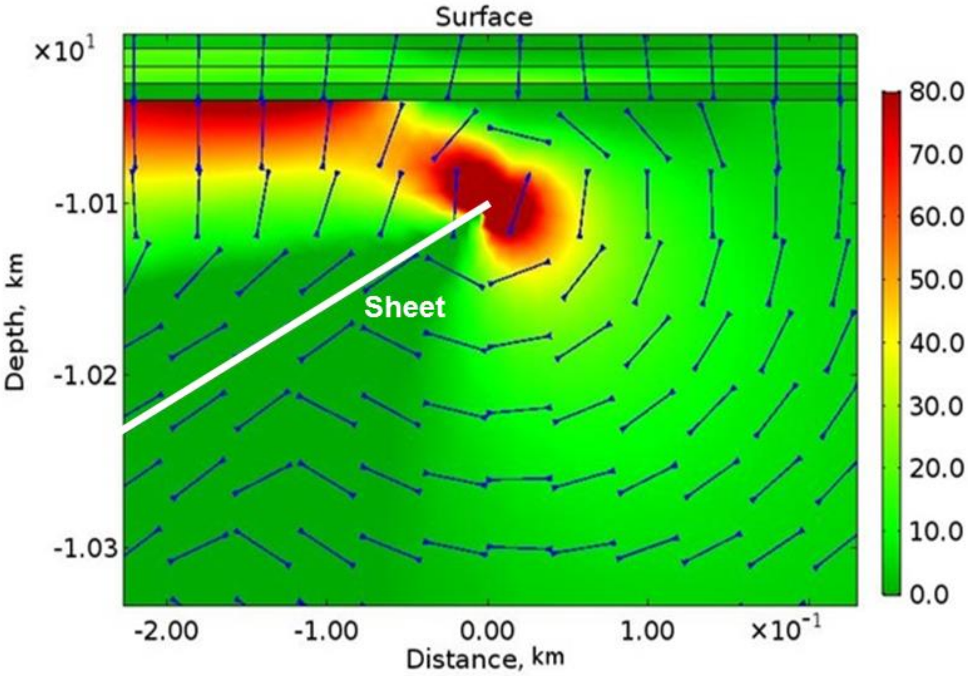


*Fig. 15. The maximum principal tensile stress ($\sigma_3$) inside the model in mega-pascals (vertical colour scale to the right of the model shows the magnitude in MPa) for a sheet dipping 30°. Layer 4 has a stiffness of 0.1 GPa.*

During magma-chamber rupture and sheet injection, the host rock is assumed to fail in a brittle manner, that is, through fracture propagation. This is in agreement with field observations which show that even close to or at the contacts with the magma chambers, rock failure during magma-chamber rupture and dike or sheet injection is predominantly brittle (Fig. 2). Many have suggested viscoelastic, plastic, and viscoplastic behaviour of the host rocks of shallow magma chambers. However, where the ruptured margins between the chambers and their host rocks can be studied in detail, the observations confirm that the failure was normally in a brittle manner (Fig. 8). The strength that needs to be reached for the magma to form an inclined sheet is the in-situ tensile strength of the roof (Eqs. 1 and 2), which is between 0.5 and 9 MPa, and most commonly 2-4 MPa (Amadei and Stephansson, 1997; Gudmundsson, 2011a,b). The in situ tensile strength is most commonly measured using small hydraulic fractures in drill-holes or wells, thereby providing a good analogy with magma-chamber rupture and sheet/dike injection.

*3.3 The driving pressure (overpressure)*

The total pressure $p_t$ and the excess pressure $p_e$, (Eqs. 1 and 2) result from and include the combined pressure effects of all the fluids (gases and liquids) in the chamber as well as any contribution of buoyancy. When either of these equations is satisfied, the chamber ruptures and an inclined sheet (or a dike) is injected into its roof or walls. The magmatic driving pressure or overpressure $p_o$ is given by (Gudmundsson, 2011a, 2020):

$$p_o = p_e + (\rho_r - \rho_m)gh + \sigma_d \tag{3}$$

where $p_e$ is the excess magmatic pressure in the chamber, $\rho_r$ is the average host-rock density, $\rho_m$ is the average magma density, $g$ is acceleration due to gravity, $h$ is the dip dimension of the sheet at a particular time during its propagation, as measured from the chamber point of rupture. The term $\sigma_d = \sigma_1 - \sigma_3$ is the differential stress at the crustal level/layer which the propagating sheet has reached at that particular time (which, for an arrested sheet, is the layer/contact hosting the sheet tip). For a feeder, the dip dimension $h$ is the vertical distance between the point of initiation at the boundary of the chamber and the Earth's surface where resulting fissure or crater cone forms.

Equation (3) can be used to estimate the magmatic overpressure of a sheet. For feeders, the overpressure follows from the aspect (length/opening) ratio of a volcanic fissure it feeds (where the opening is normally determined from GPS or InSAR data). For a sheet exposed at the surface of an eroded area, the overpressure at the time of emplacement can be estimated from the length/thickness ratio of the sheet. The following points are relevant when considering the magmatic overpressure/driving pressure (cf. Gudmundsson, 2020):

- At the time of magma-chamber rupture and sheet initiation the excess pressure $p_e$ must be positive and equal to the in-situ tensile strength of the host rock at the chamber boundary, that is, $p_e = T_0$. From Eq. (3) it follows that while $h$ is small, say for the first hundreds of metres above the chamber roof, the overpressure available to drive the sheet propagation derives primarily from the excess pressure, $p_e$. This is because for small $h$ the second term on the right-hand side of Eq. (3), the buoyancy term, does not contribute significantly to the overpressure. More specifically, for high-density basaltic sheets injected from shallow magma chambers the buoyancy may be zero, when the magma and host-rock density equal, or negative, when the magma is denser than the host rock. In both cases, the only overpressure available to drive the sheet propagation all the way to the surface is the excess pressure.

- The differential stress $\sigma_d = \sigma_1 - \sigma_3$ must be either zero or positive; it cannot be negative because, by definition, $\sigma_1$ cannot be less than $\sigma_3$. By contrast, the density difference $\rho_r - \rho_m$ can be negative, zero, or positive. The average density of the roofs of many shallow chamber (the parts of the crustal segments above the chambers, including the volcanoes themselves) is commonly similar to, or somewhat less than, that of basaltic magmas. The density difference, and thus the buoyancy term in Eq. (3), is then zero or negative, as indicated above.

- When calculating stresses around magma chambers and inclined sheets or dikes, the excess pressure (for the chamber) and the overpressure or driving pressure (for the sheet/dike) are the relevant ones and used. The total pressure is rarely used. Since excess pressure and overpressure are the pressures above $\sigma_3$ and, in the case of lithostatic state of stress, above all the principal stresses, it follows that the effect of gravity is automatically taken into account in such analyses.

### *3.4 Propagation paths*

Once the initiated inclined sheet or dike begins to propagate, the local stress field will control its propagation path. Because sheets are primarily extension fractures, as discussed in detail above, they must, by definition, follow paths that are perpendicular to $\sigma_3$ and thus parallel with the trajectories of $\sigma_2$ and $\sigma_1$. For dikes propagating in a homogeneous, isotropic crustal segment, plotting the likely paths of dikes is thus easy (Fig. 6). However, all large crustal segments, such as occur above magma chambers, are to a degree layered, that is, anisotropic and commonly heterogeneous as well. In particular, in active volcanoes and volcanic zones the mechanical properties of the layers commonly vary abruptly across contacts.

The layering or anisotropy has important implications for dike propagation paths (Geshi et al., 2010, 2012; Gudmundsson, 2011b, 2020; Philipp et al., 2013; Marti et al., 2016, 2017). The trajectories of $\sigma_1$ commonly change abruptly at contacts between mechanically dissimilar layers, resulting in complex sheet paths and sheet arrest (Figs. 7 and 8). At some contacts the trajectories of $\sigma_1$ change from vertical to horizontal or inclined, resulting in inclined sheets or dikes changing into sills/shallow-dipping sheets at contacts (Figs. 8 and 9), or becoming arrested altogether (Gudmundsson, 2020).

The layering and anisotropy to a degree thus controls the propagation paths of sheets (Figs. 7-9). But the layering has also great effects on the deformation and stresses induced by the sheets. How the mechanical layering affects sheet-induced stresses and displacement is of fundamental importance, because during unrest periods with sheet propagation we infer sheet dimensions and depth to top partly from geodetic data. Also, the likelihood of a propagating sheet reaching the surface to erupt is partly estimated from geodetic surface data. Here we present new numerical models on sheet-induced displacements and stresses, focusing on the surface effects, to which we turn now.

## 3. Model setup – software and boundary conditions

Here the finite-element-method (FEM) software Comsol Multiphysics (www.comsol.com) is used to analyse the sheet-induced displacements stresses and displacements in a mechanically layered crustal segment hosting a volcano/volcanic zone. Since inclined sheets show a great range in dip, we provide models for sheets with widely different dips, as discussed below. First, however, we give a general overview of the Comsol software.

Comsol (like other finite-element-method (FEM) programs) discretises the problem into an equivalent system of small ‘elements’ and solves simultaneous algebraic equations (Fig. 10).

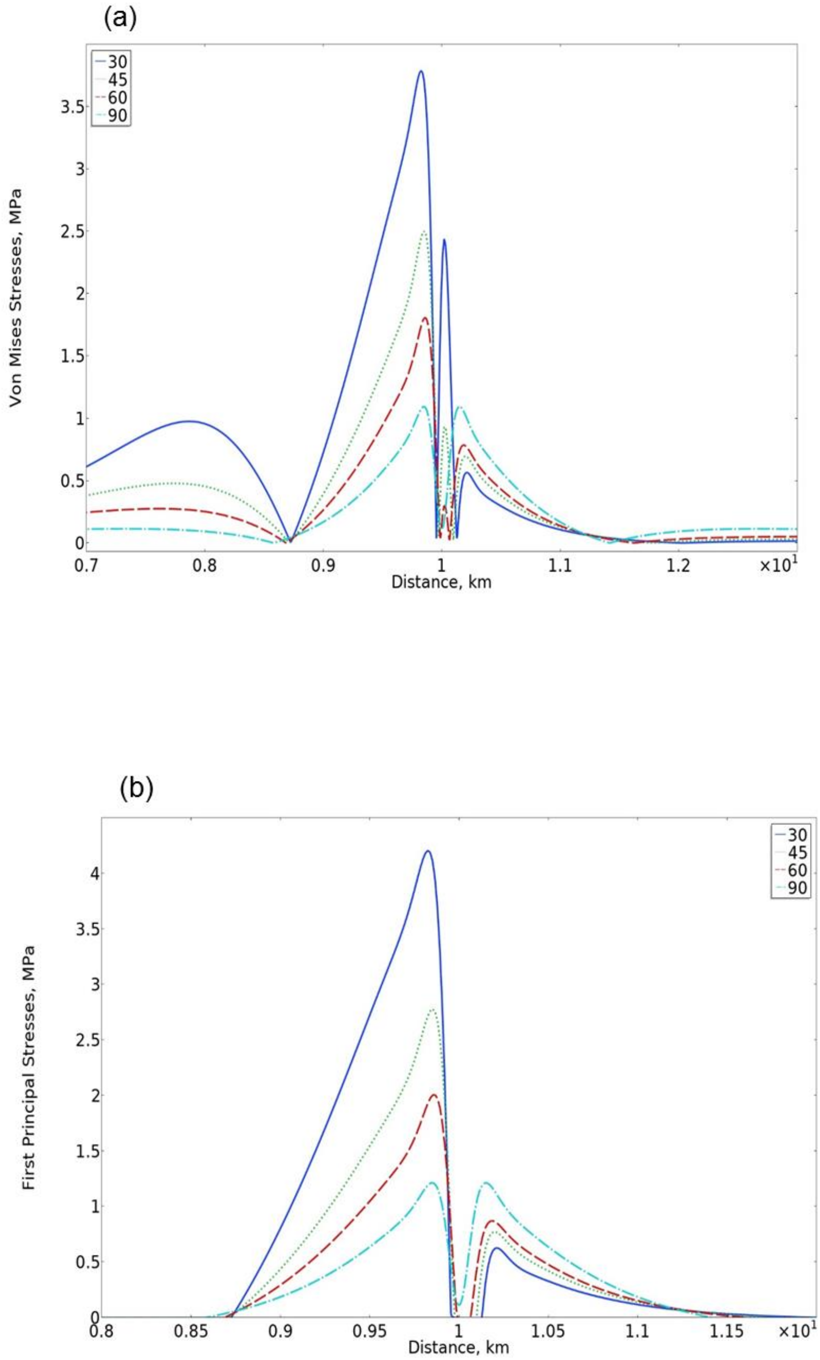

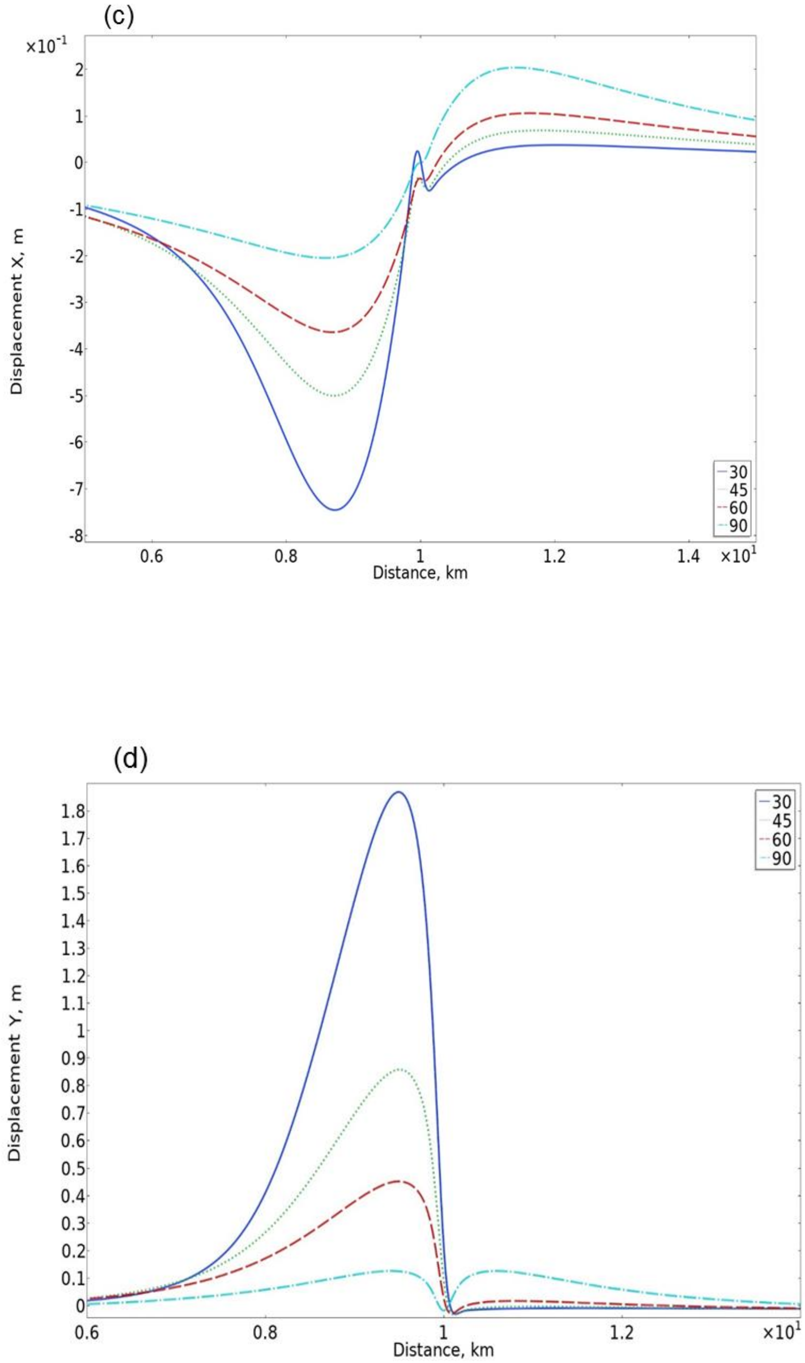


*Fig. 16. Surface stresses and displacements induced by an inclined sheet with a dip dimension of 2 km and 5 MPa internal magmatic pressure as the only loading. Layer 4 has a stiffness of 0.1 GPa. (a) Von Mises shear stress. (b) Maximum principal tensile stress ($\sigma_3$). (c) Horizontal displacement. (d) Vertical displacement.*

Then the resulting numerical approximations for each element are combined into solutions for the entire body under consideration, here a crustal segment hosting an inclined sheet. The obtained results provide approximate solutions for the differential equations that describe the problem. In calculations, loads (stresses, displacements, forces or, as here, magmatic overpressures or driving pressures) are applied at specific nodes that are normally at the corners of the elements and connect the element. From the calculated displacements at each node, the nodal stresses and the element stresses, strains, and displacements are derived using linear equations (cf. Deb, 2006; Liu and Quek, 2014).

The FEM modelling results are specific to a particular set of conditions and, therefore, give solutions only for the specified points in the body. But numerical solutions can be obtained for very complex geometries, such as anisotropic and fractured volcanoes. The FEM can additionally be applied to large strains, and heterogeneous and anisotropic mechanical properties, such as those related to the emplacement of inclined sheets in layered crustal segments and volcanoes. In the models presented here the layered crustal segment hosting the inclined sheet is discretised using triangular elements and the models are fastened in the corners, so as to avoid rigid-body rotation and translation (Fig. 10). This means that all the four corners of each model as well as at the top have zero displacement. However, all the other parts of the models are free to move, that is, can be subject to displacements in response to loading. Each model size is 20 km × 20 km and thus large enough to make the main displacements and stresses of interest and induced by the sheet unaffected by the models being fastened in the corners. More specifically, the main sheet-induced stresses and displacements are within a few kilometres of the sheet tip, and are negligible at distances of 10 km to either side of the tip (where the model is fastened).

In the models, all the layers of which the crustal segment and associated volcano are composed are assumed to behave as linear-elastic through the equilibrium and compatibility equations. This assumption derives partly from experimental physics results which show that solid rocks at crustal conditions and little strain normally behave as linear-elastic, as do volcanoes during inflation and deflation periods, all of which suggest linear-elastic behaviour to a first approximation (Scholz, 1990; Dzurisin, 2006; Segall, 2010; Gudmundsson, 2020). It follows that the numerical analysis and the modelling assume that Hook’s law of linear elasticity is valid for the behaviour of the modelled crustal segment and its layers (Gudmundsson, 2011a). Partly, however, the assumption derives from in-situ or field measurements of elastic crustal deformation around fault zones prior to earthquake ruptures. The general rock- failure criteria for the inclined sheet initiation are used (Eqs. 1 and 2), and for the propagation the condition (from Eq. 3) $p_o = T_0$ is assumed to apply. Apart from that, no specific failure criteria are used in the models because they all assume that the inclined sheet is already emplaced at the time of analysis. When estimating if the sheet-induced stresses and displacements would be large enough to cause tension fractures and/or faults, the normal shear-strength/tensile-strength criteria for the formation of these fractures are used as a basis (Gudmundsson, 2011a).

The sheet dip dimension or height is 2 km (Fig. 10). Its tip or top (where it is arrested at the time of the analysis) is at 100 m below the free surface. The surface is here assumed flat, and is thus more appropriate for a volcanic zone/field or a collapse caldera than for a volcanic edifice that stands high above its surroundings. The tip propagates no further towards the surface in the models, that is, it stays arrested at the depth of 100 m. In all the models, the only loading is the magmatic overpressure in the sheet (Eq. 3). The tensile strength of most rocks is between 0.5 and 9 MPa, the common values being 2-5 MPa (Amadei and Stephansson, 1997; Gudmundsson, 2011a). We use 5 MPa magmatic overpressure in the models. We ran all the models also for the much higher magmatic overpressure of 15 MPa. The results are geometrically similar, while the absolute stresses and displacements induced by the sheets are, as expected, higher in the models with and overpressure of 15 MPa.

The actual sheet thickness (opening) depends on the magmatic overpressure used in the models as well as the sheet dimensions and Young´s modulus (and Poisson’s ratio; here kept constant) of the host rock. The entire sheet is located within the comparatively stiff unit/layer 5 (with a Young’s modulus of 40 GPa and a Poisson’s ratio of 0.25). For a dip dimension of 2 km and an overpressure of 5 MPa, the thickness/opening would be a little under 0.5 m, and for an overpressure of 15 MPa the thickness/opening would be just over 1.4 m. As indicated above, sheet thicknesses in the range of 0.5-1.4 m are very common in sheet swarms.

Above the unit/layer hosting the inclined sheet there are 4 layers of different mechanical properties. The layers have different Young’s moduli or stiffnesses, but have all the same Poisson’s ratio of 0.25 – a common ratio for rocks (Gudmundsson, 2011a). The layers are located between the sheet tip and the surface. Each of these 4 layers has a thickness of 10 m, which remains the same in all the models. This is a common thickness of layers in lava piles such as in Iceland (e.g., Walker, 1959; Robinson et al., 1982). In most of the numerical models that we made, and all published here, the top 3 layers have constant mechanical properties. That is, their Young’s moduli and Poisson’s ratios do not change between the model runs. More specifically, the top layer (the surface layer) has a Young’s modulus of 3 GPa, the second layer a Young’s modulus of 20 GPa, and the third layer a Young’s modulus of 30 GPa. By contrast, the Young’s modulus of the fourth layer has the following values in the different runs: 0.01 GPa (very soft or compliant), 0.1 (compliant), 1 GPa (moderately stiff), and 10 GPa (stiff). Notice that the descriptions here of moderately stiff and stiff for 1 GPa and 10 GPa refer to near-surface in-situ layers. In laboratory measurements on small specimens, 1 GPa would be regarded as compliant and 10 GPa as moderately stiff (Gudmundsson, 2011a). As indicated, the unit or layer hosting the inclined sheet itself has a Young’s modulus of 40 GPa.

These are all common stiffnesses for the rocks of typical volcanoes and volcanic zones/fields (Gudmundsson, 2011a; Schaefer et al., 2015; Foged and Andreassen, 2016; Heap et al., 2020). For example, many Holocene lava flows have static Young’s moduli of the order of several mega-pascals and young pyroclastic layers may be more compliant (Heap et al., 2020). Older lava flows, such as might constitute the second and the third layer here, may have static Young’s moduli of 20-30 MPa, while others might be more compliant. Generally, the in-situ stiffness of a volcanic pile increases with depth (Heap et al., 2020). The stiffness of 40 GPa for the unit hosting the inclined sheet is similar to the estimated average static Young’s modulus of the uppermost 10 km of the volcanic rift zones in Iceland (Gudmundsson, 2003, 2011a). The Young’s moduli of the fourth layer is as low as 0.01 GPa, which is very compliant. It is, however, likely that most active volcanic zones and central volcanoes contain layers as soft as 0.1-0.01 GPa. Such zones and volcanoes normally include many layers of unconsolidated pyroclastics, such as tuff layers, and in addition many contain unconsolidated soils and sediments. Also, clays are common in some of the volcanoes, particularly in association with geothermal fields, where originally stiffer rocks have been transformed (altered) into soft clays. The normal range of Young's moduli (measured in the laboratory) of unconsolidated sand, for instance, is 0.01-0.1 GPa, that of clay is 0.003-0.5 GPa, and that of tuff 0.05-5 GPa (Gudmundsson, 2011a, 2020).

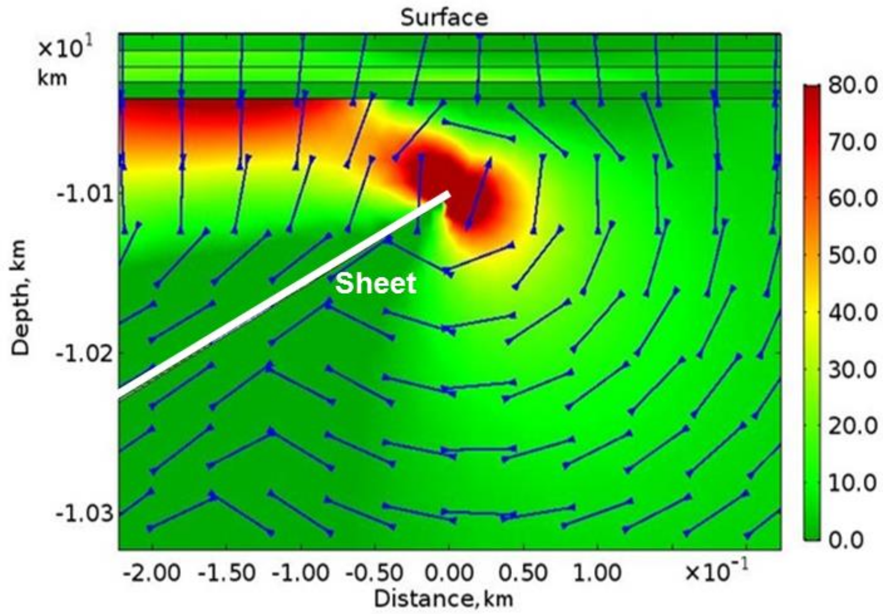


*Fig. 17. The maximum principal tensile stress ($\sigma_3$) inside the model in mega-pascals (vertical colour scale to the right of the model shows the magnitude in MPa) for a sheet dipping 30°. Layer 4 has a stiffness of 0.01 GPa.*

Apart from testing the effect of mechanical layering, particularly variation in the stiffness of the fourth layer, on the surface stresses and displacement, the models also show the effects of variation in the dip of the inclined sheets. Based on the dip measurements in numerous sheet swarms (Fig. 1), discussed above, we tested the effects of the following dips: 30°, 45°, 60°, and 90°. The last one, 90°, is for a vertical dike and is here shown as a comparison with the stresses and displacements induced by inclined sheets, most of which have dips between 30° and 60°.

In the model images presented here we zoom in on the important and relevant results. As indicated above the models are 20 km × 20 km in size, so that the model surface is 20 km wide. However, because the upper tip of the inclined sheet is so close to the surface, at 100 m, the significant stresses and displacements induced by the sheets are confined to a few of kilometres to either side of the tip, or its projection to the surface. Thus, we show the stress and displacement results only for those parts, particularly at the surface, where there are significant sheet-induced stresses and displacements. The widths of the parts where there are significant changes vary somewhat between models, but are mostly 4-8 km. Outside the central 4-8-km-wide parts shown here the models show no significant sheet-induced changes.

## 4. Numerical modelling - results

### *4.1 Layer 4 with a stiffness of 10 GPa*

In the first model layer 4 has a stiffness of 10 GPa, so similar to that of a Quaternary lava flow or a compact pyroclastic or sedimentary layer. Here we first show the magnitude of $\sigma_3$, for the sheet dips 30°, 45°, and 60° (Fig. 11). For the surface stresses we also show, for comparison, the results for a dike dipping 90°, while more detailed dike results are given by Al Shehri and Gudmundsson (2018) and by Bazargan and Gudmundsson (2019). The results show that even if layer 4 is reasonably stiff (10 GPa), it still suppresses the tensile stress, so that the stress is transferred instead to other layers – in particular, to layers 2 and 3. Furthermore, the tensile stress close to and at the contact between the unit/layer (40 GPa) hosting the sheet is raised (concentrated).

The theoretical tensile stress exceeds 40 MPa around the tip of the sheets for all sheet dips, but is as high as 80 MPa for the sheets dipping 45° and 30° (Fig. 11a,b). So high tensile stresses would not be reached in nature – the rock would fracture once the in-situ tensile strength was reached (normally several mega-pascals). The stress distribution is also highly asymmetric, the zone of high stress being primarily to the left of the tip of the sheet. This follows because the dip (inclination) of the sheet is to the left, so that the loaded crustal segment between the sheet and the bottom of layer 4 is much smaller and narrower, and thus takes on higher stress, than the segment to the right of the sheet. For the same reason, high tensile stress in layers 2 and 3 occurs only in the upper left part of the loaded crustal segment.

The ticks indicate the trajectories or orientation of $\sigma_1$. They give a crude indication of the likely orientation of the next propagation step that a sheet would take in case it propagated further. Notice that the ticks are just a crude indication of the orientation of such a step, and following the next step (if it happened, which is not the case here, given that the sheet is assumed arrested) the local stress field, hence the orientation of the $\sigma_1$, would change somewhat. In the present paper, we show the ticks of $\sigma_1$ so as to make the stress information more complete, but they are not very relevant to the main discussion, which focuses on the sheet-induced surface stresses and displacements.

The surface stresses and displacements associated with the sheet models in Fig. 11 are shown in Fig. 12. Here and elsewhere in the surface stress and displacement models the projection of the tip of the inclined sheet meets the surface at a distance of 10 km from either margin of the model, that is, in the centre of the model. Notice that the horizontal distances (along the horizontal or X-axis) in all the figures is given as a number multiplied by 10 (shown as $10^1$). This means, for example, that the distance of 1 km corresponds to $1 \times 10^1$ km = 10 km, which is the centre of the model.

The largest surface von Mises shear and tensile ($\sigma_3$) stresses exceed 6 MPa (Fig. 12a,b) and are induced by the sheet dipping at 30°. Since the common in-situ tensile strength is 2-4 MPa and the shear strength 4-8 MPa, these stresses would result in fracture formation, particularly in the formation of tension fractures. All the surface stresses are asymmetric about the projection of the tip of the sheet to the surface (subsequently referred to as the 'tip of the sheet') except for the dike dipping 90°. As expected, the shear stress (Fig. 12a) is somewhat less 'asymmetric' than the tensile stress (Fig. 12b). The tensile stress ($\sigma_3$) peaks to the left of the tip of the sheet (above the dipping sheet) are highest for the sheet dipping 30°, and then gradually diminish until they reach the lowest values for the vertical dike (Fig. 12b). By contrasts, to the right of the sheet tip, that is, in the direction opposite to the dip direction of the sheet, the tensile stress associated with the dike is the highest.

The variation in the shear stress magnitudes at the surface is generally more complex than those of the tensile stress magnitudes (Fig. 12a). This is partly because the shear stress is a function of both $\sigma_3$ and $\sigma_1$. The highest shear stress is, again, for the 30° dipping sheet, and peaks on both sides of the sheet tip. But the shear stress for the 45° dipping sheet is also higher, on both sides, than that of the vertical dike. In addition, there is a small additional peak in the shear stress for the 30° dipping sheet to the left, in the down-dip direction of the sheet. This, 'peak', however, reaches only about 1 MPa and would normally not be high enough shear stress to induce faulting.

The horizontal (Fig. 12c) and vertical (Fig. 12d) displacements induced by the sheet are also highly asymmetric about the tip of the sheet. For the horizontal displacements, the negative values (to the left of the tip) simply mean displacements to the left, that is, in the dip direction of the sheet, whereas the positive values mean horizontal displacement to the right, that is, in the opposite direction. All the displacements are shown as fraction of metre, that is, as $10^{-1} = 0.1$ times the values in metres. Thus, -5 on the vertical scale is $-5 \times 10^{-1}$ m = 0.5 m = 50 cm. All the displacements are asymmetric across the sheet tip, except those induced by the dike.

The maximum horizontal displacement is for the 30° dipping sheet, occurs about 1.2 km to the left of the sheet tip (down-dip direction) and reaches 0.8 m (Fig. 12 c). For comparison the maximum displacement induced by the dike, is only about 0.2 m. All the displacements to the left of the sheet tip are much larger than those on to the right of the sheet tip (except for the dike, where the displacements are equal).

The maximum vertical displacement, also induced by the 30° dipping sheet, occurs about 0.6 km to the left of the sheet tip (down-dip direction) and reaches about 1.70 m. The sheet here it generates space for itself primarily by uplift or doming of the surface above. This is to be expected when the sheet is very shallow (the tip is at the depth of only 100 m) and gently dipping (30°). For the other sheet dips the maximum uplift is much less, namely about 0.8 m (for 45° dipping sheet), about 0.4 m (for 60° dipping sheet), and 0.1 m (for vertical dike). These are somewhat larger than the maximum horizontal displacements, except for the dike where the horizontal displacement (about 0.2 m in each direction) is somewhat larger than the dike-induced vertical displacement. The lateral distance to the uplift peaks is also less for these than for the 30° dipping sheet. Apart from about 0.1 m uplift induced by the dike, there are no significant vertical displacements induced by the sheet to the right of its tip.

*4.2 Layer 4 with a stiffness of 1 GPa*

Here we show only the internal tensile magnitude of $\sigma_3$ and the trajectories of $\sigma_1$ for the sheet dipping 30° (Fig. 13). The trajectories of $\sigma_1$ are here similar to those in Fig. 11a but there is less tensile stress concentrates here in layers 2 and 3. This follows because layer 4 in the model in Fig. 11a has a stiffness of 10 GPa and therefore transmits stresses more easily to the

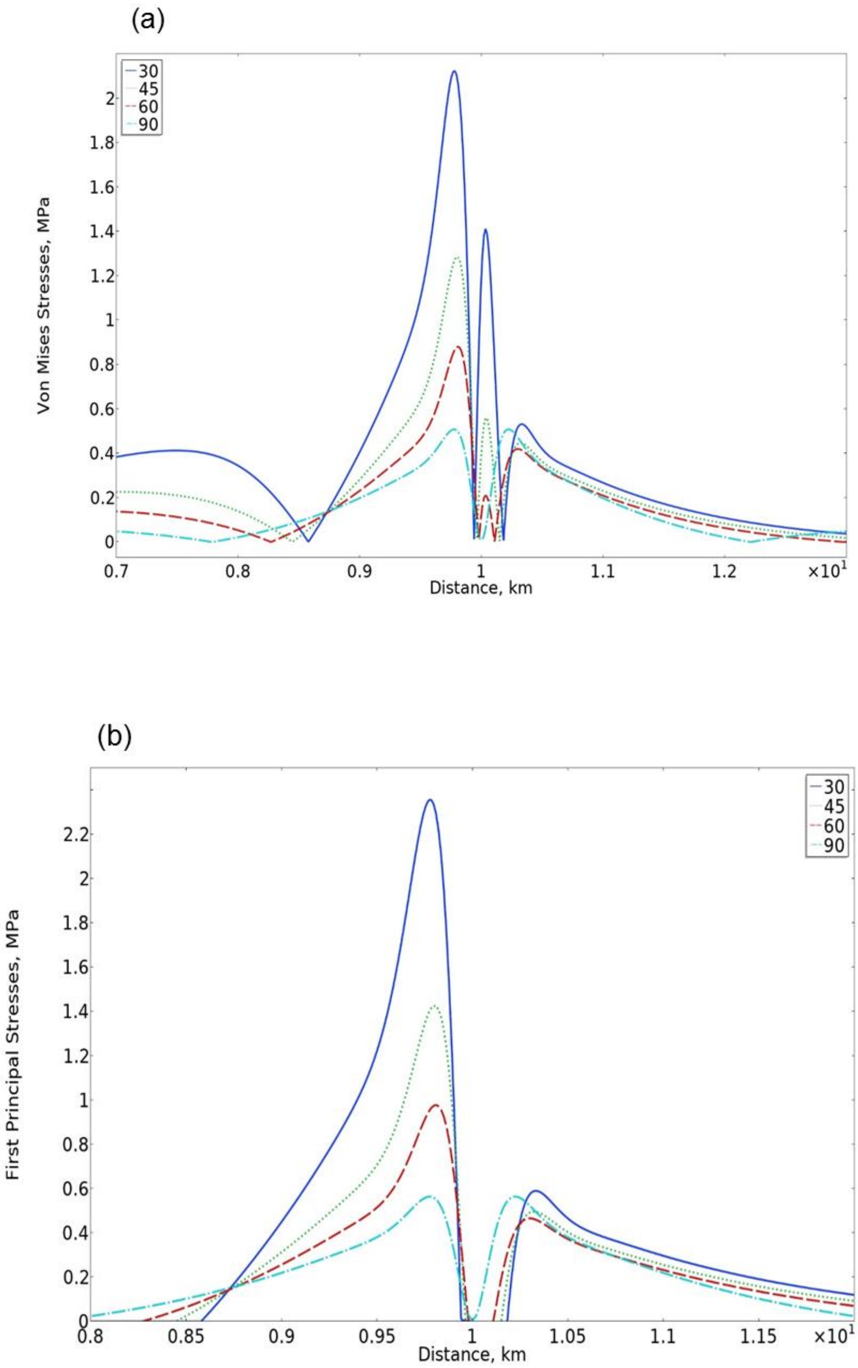

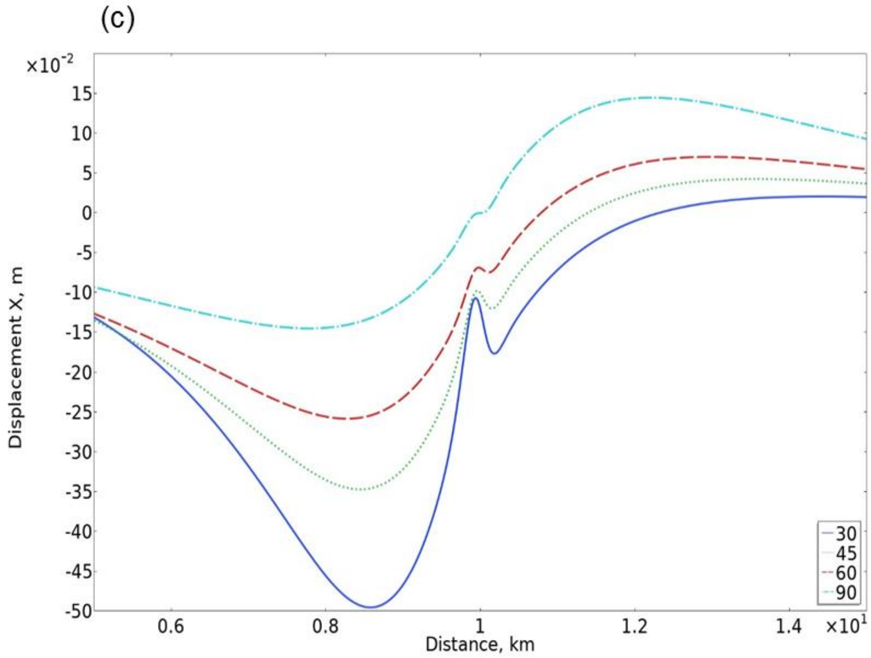


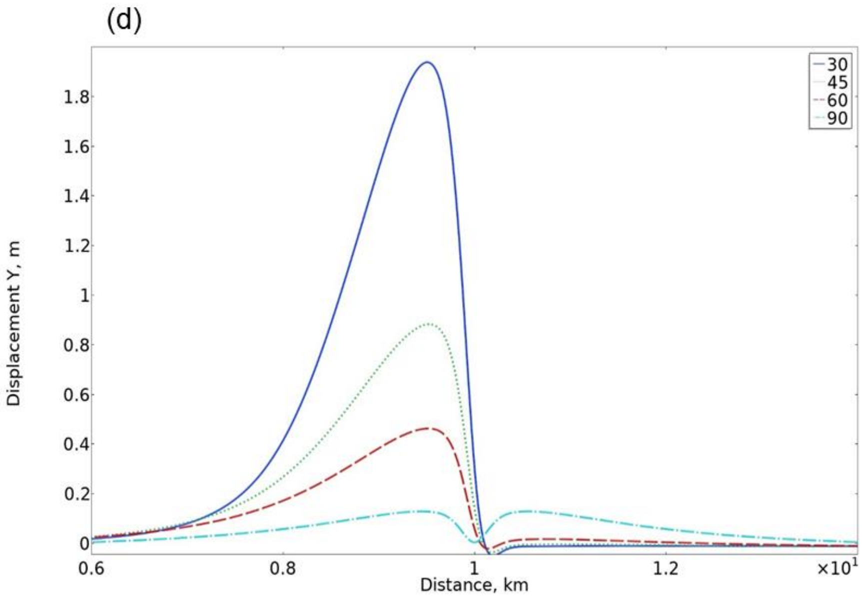


*Fig. 18. Surface stresses and displacements induced by an inclined sheet with a dip dimension of 2 km and 5 MPa internal magmatic pressure as the only loading. Layer 4 has a stiffness of 0.01 GPa. (a) Von Mises shear stress. (b) Maximum principal tensile stress ($\sigma_3$). (c) Horizontal displacement. (d) Vertical displacement.*

layers above, layers 2 and 3, than in the present model where layer 4 has the much lower stiffness of 1 GPa. As a consequence, in the present model the tensile stress becomes more concentrated below the lower margin of layer 4, that is, in the top part of the unit hosting the sheet. In this top region above the sheet (to the left of the sheet tip) the theoretical tensile stress reaches 80 MP. This is higher than in the previous model (Fig. 11a) where the 80 MPa is reached only around the tip itself but not below the contact between layer 4 and the layer hosting the sheet. So high tensile stresses cannot be reached in nature; the rock fails commonly at tensile stresses of 2-4 MPa as discussed above.

The surface shear (Fig. 14a) and tensile (Fig. 14b) stresses are again highest for the sheet dipping 30°. The stress peaks, however, are somewhat lower than those in Figs. 12a and 12b. This is primarily because the comparatively compliant layer 4 of 1 GPa transmits less stresses to the surface that the stiffer layer 4 (10 GPa) in the model in Fig. 12. Nevertheless, for the 30° dipping sheet the peak shear stress is about 5.3 MPa (Fig. 14a) and the peak tensile stress around 5.8 MPa (Fig. 14b). Normally, so high surface stresses would result in fracture formation, or reactivation of existing fractures. In particular, the tensile $\sigma_3$ is so high that it would almost certainly generate tension fractures. As before, all the stresses are asymmetric with the exception of those induced by the dike.

The maximum horizontal displacement is again for the 30° dipping sheet and reaches 0.81 m (Fig. 14c). It is noticeable that the horizontal displacements on to the left of the sheet tip are here somewhat larger, and those to the right of the sheet tip somewhat smaller, than those in the earlier model (Fig. 12c). Overall, however, the horizontal displacement values are similar for all the sheet dips to those in the earlier model (Fig. 12c).

The maximum vertical displacement is, as before, for the 30° dipping sheet and reaches about 1.76 m (Fig. 14d), or slightly larger than in the previous model (Fig. 12d). This very slight increase is due to layer 4 being more compliant in this model than in the previous one. Similar slight increase is seen in the maximum displacements for the other dips of the sheet. As before, all the displacements are highly asymmetric about the tip of the sheet except for the dike.

### *4.3 Layer 4 with a stiffness of 0.1 GPa*

The trajectories of $\sigma_1$ are again similar to those in the earlier models (Figs. 11a and 13), but there is much less tensile stress concentrates in layers 2 and 3 (Fig. 15). This is the result of layer 4 being soft (0.1 GPa) and thus transmitting little tensile stress to layers 2 and 3 (and to the surface, as discussed below). Consequently, the zone of high tensile stress concentration – in excess of 80 MPa – below the bottom of layer 4 is here much larger than in the model in Fig. 13. Tension fractures would be expected to develop in this zone.

As before, the surface shear (Fig. 16a) and tensile (Fig. 16b) stresses are highest for the sheet dipping 30°. The stress peaks, however, are much lower than those in Figs. 12a,b and 14a,b. The difference is primarily because of compliant layer of 0.1GPa which transmits little stress to the surface. For the 30° dipping sheet the peak shear stress is about 3.8MPa (Fig. 16a) and the peak tensile stress around 4.2MPa (Fig. 16b). Neither of these stresses does necessarily result in fracture formation, but both could reactivate existing fractures. The tensile $\sigma_3$, at over 4 MPa, however, is so high that it could generate tension fractures. Again, all the stresses are asymmetric with the exception of those induced by the dike.

The maximum horizontal displacement for the 30° dipping sheet is about 0.74 m and occurs, as before, to the left of the sheet tip (Fig. 16c), whereas the displacement to the right of the tip is about 0.02 m (2 cm). Thus the trend continues with increasing compliance of layer 4 that the horizontal displacement on to the left of the sheet tip increases whereas the displacement to the right of the sheet tip decreases.

The maximum vertical displacement for the 30° dipping sheet reaches about 1.89 m (Fig. 16d), and thus significantly larger than in the previous models. Similar increases occur in the maximum displacements for the other dips of the sheet. All the displacements are highly asymmetric about the tip of the sheet except for the dike.

### *5.4 Layer 4 with a stiffness of 0.01 GPa*

Again the trajectories of $\sigma_1$ are similar to those in the earlier models (Figs. 11a, 13, and 15), but very little tensile stress concentrates in layers 2 and 3 (Fig. 17), primarily because layer 4 is now so soft (0.01 GPa) that it transmits very little tensile stress to layers 2 and 3 and the surface. The zone of high tensile stress concentration – in excess of 80 MPa – below the bottom of layer 4 is here large and would be expected to develop tension fractures.

Again the surface shear (Fig. 18a) and tensile (Fig. 18b) stresses are highest for the sheet dipping 30°. The stress peaks, however, are much lower than those in Figs. 12a,b, 14a,b, and 16a,b. The difference is primarily because of the very compliant layer of 0.01GPa which transmits little stress to the surface. For the 30° dipping sheet the peak shear stress is about 2.2 MPa (Fig. 18a) and the peak tensile stress around 2.3MPa (Fig. 18b). Neither of these stresses is likely to generate fractures, but could possibly reactive some fractures. As before, all the stresses are asymmetric with the exception of those induced by the vertical sheet, the dike.

The maximum horizontal displacement for the 30° dipping sheet is about 0.49 m and occurs, as before, to the left of the sheet tip (Fig. 18c). The displacement to the right is now negative, about 0.01 m (1 cm), that is, is towards the left (towards the sheet tip rather than away from the tip as in earlier models). This displacement stays negative out to a distance of about 2 km to the right of the sheet tip, where it becomes positive (to the right and away from the tip) again. In fact, the horizontal displacements to the right of the sheet tip are all negative (are towards the tip) for a while except that of the dike. There were also some negative displacements in this sense in the model in Fig. 16.c, but of a much smaller magnitude and extension.

The maximum vertical displacement for the 30° dipping sheet reaches about 1.95 m (Fig. 18d), and thus the largest one in all the models. Similar increases occur in the maximum displacements for the other sheet dips. All the displacements are highly asymmetric about the tip of the sheet except for the dike.

## 5. Discussion

There have been very few analytical and numerical studies of the stress and displacement fields induced by inclined sheets. Those few that exist are mostly based on modelling the sheets as elastic dislocations. The models are then applied to invert surface geodetic data to infer the opening or thickness, strike, dip, and depth of the inclined sheets, and can also be applied to dikes and sills. The elastic dislocation theory as applied to volcano deformation in general is reviewed in detail by Okada (1985, 1992), Dzurisin (2006), and Segall (2010). In the dislocation theory it is normally assumed that the volcano/crustal segment hosting the inclined sheet act as a homogeneous, isotropic, elastic half-space. It follows that the models do not consider any effects of mechanical layering or contacts between layers on the sheet-induced stresses and deformation. Most models that consider layering are numerical and have, so far, generally been confined to the stresses and displacements induced by vertical dikes (e.g., Gudmundsson and Brenner, 2001; Gudmundsson, 2003; Gudmundsson and Loetveit, 2005; Al Shehri and Gudmundsson, 2018; Bazargan and Gudmundsson, 2018). Analytical and numerical dike models are reviewed by Rivalta et al. (2015) and by Townsend and Pollard (2017).

A representative example of inclined sheets (and dikes) modelled as elastic dislocations is provided by Dzurisin (2006). Here the dislocation models show the vertical (Fig. 19a) and the horizontal (Fig. 19b) displacements induced by a sheet dipping at 0° (a sill), 60° (an inclined sheet), and at 90° (a dike). In addition, the author shows the same for a classical Mogi model, that is, a nucleus of strain. The results are geometrically generally similar to those shown in the models in the present paper (Figs. 12, 14, 16, and 18). In particular, the following geometric similarities are noticeable:

- The vertical displacement induced by the dike (90° dip) has a clear 'valley' shape. That is, the displacement is zero or negative (subsidence) right above the dike (above its tip) and then forms positive peaks on either side (compare Figs. 12d, 14d, 16d, and 18d with Fig. 19a). More detailed results on the displacement associated with a dike in a layered crust are provided by Bazargan and Gudmundsson (2019).
- The vertical displacement induced by the 60° dipping sheet shows a steep downward slope above the tip of the sheet and becomes somewhat negative for a short while to the right of the tip and then close to zero (compare Figs. 12d, 14d, 16d, and 18d with Fig. 19a).
- The horizontal displacement induced by the dike is the same on either side of the vertical y-axis except for a change in sign. The displacement is zero right above the tip of the dike (compare Figs. 12c, 14c, 16c, and 18c with Fig. 19b).
- The horizontal displacement induced by the 60° dipping sheet shows a noticeable 'wave' immediately to the right of the vertical y-axis, that is, after crossing the tip of the sheet (compare Figs. 12c, 14c, 16c, and 18c with Fig. 19b). The absolute location of the 'wave', however, depends on the layering; in the present models on the stiffness of layer 4.

There are, however, many differences in detail between the models presented here - and in Al Shehri and Gudmundsson (2018) and Bazargan and Gudmundsson (2019) – and those presented in Fig. 19. The latter, being based on elastic half-space modelling, ignore the effects of layering in volcanoes/volcanic zones. The present models show that when layering is taken into account, the details of the magnitude (size) and the geometry of the displacement curves change. This is particularly clear for the horizontal displacement which decreases much as the stiffness of layer 4 decreases (Figs. 12c, 14c, 16c, and 18c). The uplift or vertical displacement is also affected, but to a lesser degree (Figs. 12d, 14d, 16d, and 18d).

In addition, the present models show that the stresses induced by the sheet depend strongly on the layering. This is clear from the distribution and magnitude of the maximum

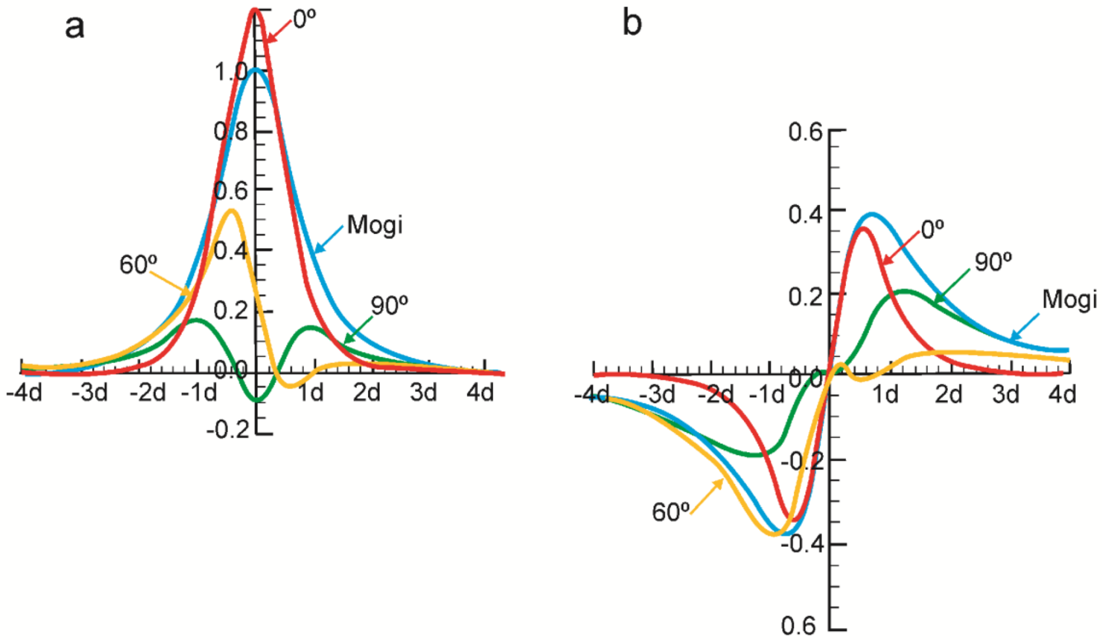


*Fig. 19. Surface displacements induced by inclined sheets (and dikes) modelled as elastic dislocation and dipping at 0° (a sill), 60° (an inclined sheet), and at 90° (a dike). Induced (a) vertical and (b) horizontal surface displacements. In addition, the author shows the same for a classical Mogi model, that is, a nucleus of strain (modified from Dzurisin, 2006).*

tensile stress inside the volcano/crustal segment (Figs. 11, 13, 15, and 17). Soft layers allow little stress to be transmitter to the layers above – here layers 2 and 3. And, most importantly, soft layer 4 greatly reduces the shear and tensile stress that is transmitted to the surface (Figs. 12, 14, 16, and 18). As the stiffness of layer 4 decreases from 10 GPa to 0.01 GPa, the maximum shear stress at the surface decreases from about 6.6 MPa to 2.2 MPa (Figs. 12a and 18a) and the maximum tensile stress from about 6.9 MPa to about 2.3 MPa (Figs. 12b and 18b). This means that, even with only one comparatively thin (10 m) soft layer close to the surface of a volcano/volcanic zone (and such layers are very common, almost universal), there is a great reduction in the maximum sheet-induced stresses at the surface, and thereby in the likely fracture formation induced by the sheet.

To test the size of the effect of layering on sheet-induced stresses and displacements we made an elastic half-space model of exactly the same sheet configurations and loading (5 MPa overpressure) as in our layered models. The exact stress and displacement fields in the half-space model depend on the selected elastic properties. Because the sheet is very shallow, we use a uniform Young's modulus of 20 GPa in the half-space model (Fig. 20). This is an appropriate average value for the uppermost part of the crust in active volcanic zones/fields zones and central volcanoes (Gudmundsson, 2020). As in all the layered models, we use a uniform Poisson's ratio of 0.25.

The results for the elastic half-space model (Fig. 20) are widely different from those of all the layered models. In particular, in the half-space model the sheet-induced surface stresses (Fig. 20a,b) and displacements (Fig. 20c,d) and much larger than in any of the layered models (Figs. 12, 14, 16, and 18). For example, for a sheet dipping 30° the maximum surface stresses in the half-space model are about 57 MPa, for the shear stress (Fig. 20a) and 63 MPa for the tensile stress (Fig. 20b), whereas for the layered models the maximum surface stresses are 6.6 MPa for the shear stress and 6.9 MPa for the tensile stress (Figs. 12a and 12b). As indicated above, these maximum values are for layer-4 stiffness of 10 GPa. In the half-space model the maximum horizontal displacement induced by a sheet dipping 30° is close to 1.5 m (Fig. 20c) and the maximum vertical displacements about 3 m (Fig. 20d). The maximum induced horizontal displacement in the layered models by a sheet dipping 30° is about 0.8 m and occurs when layer 4 has a stiffness of 1 GPa (Fig. 14c). By contrast, the maximum vertical displacements in the layered models for a sheet dipping 30° is 1.95 m and occurs when layer 4 has a stiffness of 0.01 GPa (Fig. 18d).

To test the difference between half-space and layered models further, we also ran half-space models with stiffness (Young's modulus) different from that above (20 GPa). In particular, we made one half-space model with uniform stiffness of 40 GPa and another with uniform stiffness of 10 GPa. The results (not illustrated) are as follows. The maximum surface stresses induced by a sheet dipping 30° are about 57 MPa for the shear stress and about 63 MPa for the tensile stress in both half-space models, that is, the model with stiffness of 40 GPa and 10 GPa. The maximum induced surface displacements for the sheet dipping 30°, however, differ widely between the models. For the model with a stiffness of 40 GPa the maximum induced horizontal surface displacement is close to 0.7 m, whereas the maximum vertical displacement is just over 1.6 m. By contrast, for the model with a stiffness of 10 GPa the maximum induced horizontal surface displacement is close to 3 m, and the maximum vertical displacement about 6 m. On comparison with the 20 GPa half-space model, we see that the maximum induced surface stresses in all the half-space models remain the same, whereas the surface displacements gradually increase as the uniform stiffness decreases from 40 GPa to 20 GPa, and then to 10 GPa. Furthermore, and most importantly here, the maximum induced surface stresses are much larger, and horizontal and vertical surface displacements considerably larger, in all the elastic half-space models than in any of the layered models.

These results are agreement with earlier results on dike-induced stresses in elastic half-spaces and layered crustal segments. Al Shehri and Gudmundsson (2018) compared induced stresses by dikes in elastic half-spaces (uniform Young's modulus of 40 GPa and a Poisson's ratio of 0.25) with those induced by dikes, of the same dimensions, depth-to-tip, and overpressure (here 6 MPa), in crustal segments with layers of different mechanical properties. For the surface shear and tensile stresses, the results show that even a single moderately stiff layer greatly reduces the induced surface stresses. The shallowest dike tips considered in the models by Al Shehri and Gudmundsson (2018) are 300 m below the surface. In the half-space model, the dike with a tip at this depth induces maximum surface tensile and shear stresses of about 18 MPa. When a moderate layering is introduced, with all the layers being moderately stiff (Young's modulus of 17-27 GPa), however, the maximum surface stresses are reduced to about 9 MPa. When the layer just above the tip of the dike is soft, such as a compliant sedimentary or pyroclastic layer (Young's modulus of 1 GPa), the dike-induced surface stresses are reduced to about 2 MPa.

Thus, the half-space models tend to overestimate the induced stresses for a given dike/sheet geometry and loading conditions. It follows that half-space models normally overestimate of the depth to the upper tip (top) of the dike/sheet and underestimate of the dike/sheet thickness. For example, Al Shehri and Gudmundsson (2018) concluded that when reasonable layering was taken into account for the dike emplaced in Saudi Arabia during a 2009 volcanotectonic the dike tip most likely became arrested at a depth of a few hundred

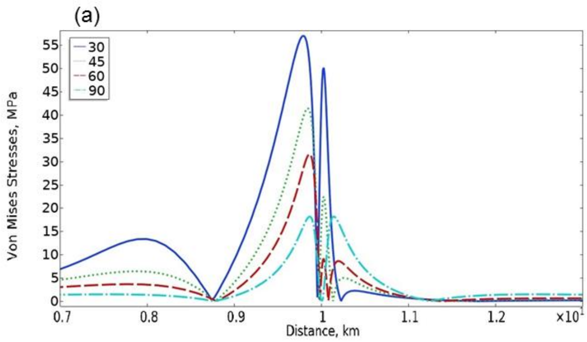


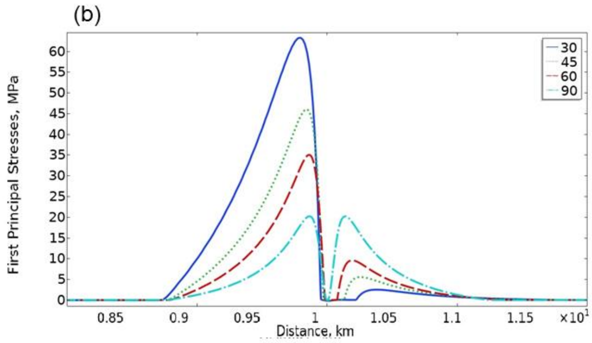

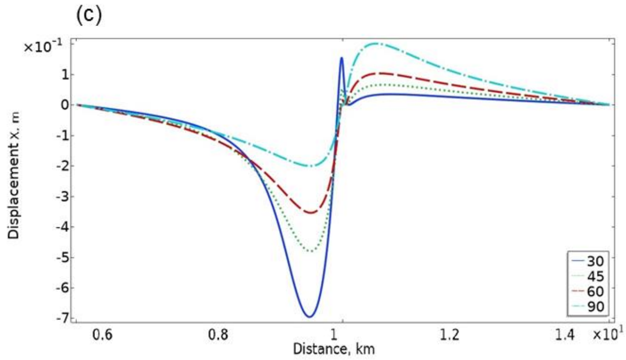


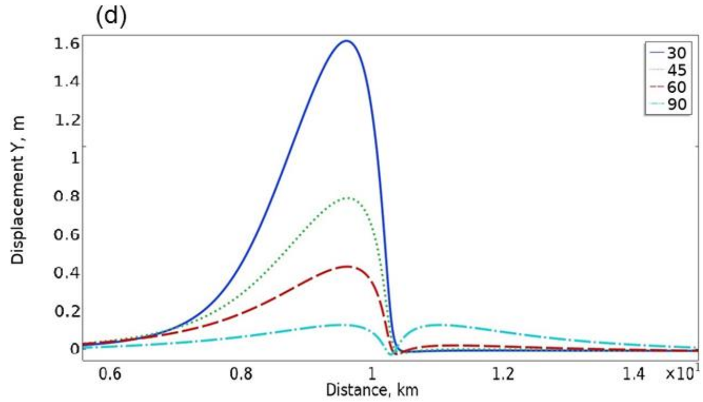


*Fig. 20. Surface stresses and displacements induced by an inclined sheet with a dip dimension of 2 km and 5 MPa internal magmatic pressure as the only loading. The tip (top) of the sheet is at 100 m below the free surface of an elastic half-space with a uniform Young's modulus (stiffness) of 20 GPa. (a) Von Mises shear stress. (b) Maximum principal tensile stress ($\sigma_3$). (c) Horizontal displacement. (d) Vertical displacement.*

metres below the surface and had a thickness of 6-12 m. By contrast, elastic half-space models for the same dike indicated a dike thickness of about 2 m and the depth of dike-tip arrest of 1-2 km. Thus, generally, layering should be taken into account in models trying to infer the dimensions and depth to top of arrested dikes and inclined sheets based on surface deformation.

This follows because active volcanoes and volcanic zones/fields are known to contain numerous compliant layers, particularly close to the surface. These are easily seen in the field in caldera walls, pit crater walls, landslide walls, fault walls, sea cliffs, and other erosional and tectonic sections into volcanoes, as well as in numerous drill holes into volcanoes. From such sections it is commonly easy to estimate roughly the mechanical layering in the upper parts of volcanoes/volcanic zones. In the absence of exact information about the layering in a given volcano undergoing unrest, generalised layering based on information from similar volcanoes can be used in the stress and displacement modelling. Taking the layering into account in modelling sheet (and dike) injection – so as to estimate the likely dimensions, depth, and other geometric factors of the intrusions – are a necessary step in order to improve our understanding of unrest periods with sheet injections.

The present models (compare Figs. 12b, 14b, 16b, 18b, and 20b with 12d, 14d, 16d, 18d, and 20d) show that the locations of the maximum surface uplift or vertical displacement and the horizontal displacement do not coincide with the locations of the maximum (peak) surface tensile and shear stresses. More specifically, the maximum stresses are much closer to the sheet tips than the maximum horizontal or vertical displacements. For example, the maximum tensile stress for the 30° dipping sheet when layer 4 has a stiffness of 1 GPa is at about 0.17 km to the left of the tip of the sheet (Fig. 14b) whereas the maximum vertical displacement for the same model is at 0.6 km from the tip. Similar differences between displacement peaks and stress peaks occur for other sheet dips.

It is important to remember that the most likely fracture formation is normally not where the displacement peaks occur but rather where the stress peaks occur. These results are in agreement with earlier modelling and observational results (Al Shehri and Gudmundsson, 2018; Bazargan and Gudmundsson, 2019) and are particularly important when trying to understand surface deformation in relation to injected sheets during unrest periods in volcanoes.

The results of all the models (Figs. 11-18) indicate the importance of the effects of mechanical layering in volcanoes/volcanic zones on sheet-induced displacements and stresses. The models show that a single compliant layer may reduce the sheet-induced surface stresses so much as to make surface fracturing unlikely until the sheet has more or less reached the surface. This is in agreement with the field observations of arrested sheet (particularly dike) tips which show that sheets arrested at shallow depths commonly do not generate tension fractures or normal faults above their tips (Al Shehri and Gudmundsson, 2018; Bazargan and Gudmundsson, 2019; Gudmundsson, 2020).

## 6. Conclusions

The main conclusions of this paper may be summarised as follows:

- The new numerical results presented here focus on the effects of mechanical layering on sheet-induced stresses and displacements, primarily at the surfaces of central (polygenetic) volcanoes and volcanic zones/fields. The models use 5 layers with different mechanical properties, that is, different stiffnesses or Young's modulis. In the models the surface layer, layer 1, has a stiffness of 3 GPa, the next layer below, layer 2, a stiffness of 20 GPa, and layer 3 a stiffness of 30 GPa. Each of these layers is 10 m thick. Below layer 4 is layer or unit 5, with a stiffness of 40 GPa, which hosts the inclined sheet. The sheet is 0.5-1.4 m thick (depending on the magmatic overpressure), with a dip dimension 'length' (in a vertical section) of 2 km, and an arrested tip at 100 m below the surface. These are common dimensions of inclined sheets in swarms in Iceland, Scotland, the Canary Islands, and elsewhere.

- Between model runs, the stiffness of layer 4 is varied, from 10 GPa, and thus rather stiff, to 1 GPa, 0.1 GPa, and 0.01 GPa. The last stiffness, 0.01 GPa, is very compliant but layers of similar stiffness are likely to occur in most active central volcanoes and volcanic zones. The modelled sheets have four dips: 30°, 45°, 60°, and 90°, the last one being a vertical dike. These dips span the common dip range of sheets in sheet swarms, based on observations in Iceland, Scotland, the Canary Islands, and elsewhere.
- The internal stress shown as contours is the maximum tensile stress, $\sigma_3$ (Figs. 11, 13, 15, and 17). The results show clearly the importance of mechanical layering. In particularly, when layer 4 becomes more compliant, less and less stress is transmitted to the layers above (layers 2 and 3) and to the surface (layer 1). By contrast, the tensile stress concentrates at the top of layer 5, at its contact with layer 4, and is so high that fracturing would be expected.
- For the various dips of the sheets, the following sheet-induced surface results are provided. (a) The von Mises shear stress, (b) the principal tensile stress ($\sigma_3$), (c) the horizontal displacement, and (d) the vertical displacement.
- The sheet dipping 30° induces the greatest surface stresses and displacements. Both stresses and displacements are highly asymmetric across the tip of the sheet, except for the vertical sheet (the dike), where they are symmetric. When the stiffness of layer 4 decreases to 0.1 GPa and 0.01 GPa, little stress is transmitted to the surface, so that the surface stresses gradually decrease. For this decrease in stiffness, changes in vertical displacement, however, are comparatively small but greater for the horizontal displacement.
- In particular, when the stiffness of layer 4 decreases from 10 GPa to 0.01 GPa, the maximum shear stress at the surface decreases from about 6.6 MPa to 2.2 MPa (Figs. 12a and 18a) and the maximum tensile stress from about 6.9 MPa to about 2.3 MPa (Figs. 12b and 18b). Thus, even a single comparatively thin (10 m) soft layer close to the surface of a central volcano/volcanic zone (and such layers are almost universal), there is a great reduction in the maximum sheet-induced stresses at the surface, and thereby in the likelihood of fracture formation.
- Three elastic half-space models (each with a uniform Young's modulus) were made of exactly the same sheet geometries and loading conditions. The results show that the sheet-induced surface displacements gradually decrease as the uniform Young's modulus is decreased from 40 GPa (first model) to 20 GPa (second model; Fig. 20),

and then from 20 GPa to 10 GPa (third model), whereas the induced surface stresses remain similar. Most importantly, however, the maximum induced surface stresses are much larger, and horizontal and vertical surface displacements considerably larger, in all the three elastic half-space models than in any of the layered models. This, again, indicates that reasonable layering must be taken into account when analysing measured displacement fields induced by sheets/dikes during unrest periods.

- The stress peaks and displacement peaks do not coincide. Tension fractures and faults – in particular the boundary faults of grabens – are most likely to form, if at all, at the location of the tensile/shear stress peaks and not, as is commonly suggested, at the location of the surface uplift peaks.
- Information on mechanical layering in active volcanoes is widely available, from eroded cliff sections, caldera walls, pit-crater walls, landslide walls, fault walls, and drill holes. Reasonable estimates of the variation in stiffness of the layers can thus commonly be made for active volcanoes. As indicated above, the results suggest that failure to take typical and reasonable mechanical layering in central volcanoes and volcanic zones into account, such as by using homogeneous, elastic half-space dislocation models, when inferring sheet geometries and depths thorough the inversion of surface-deformation data is likely to lead to highly unreliable results. In particular, such models tend to underestimate the dike/sheet thickness and overestimate the theoretical sheet-induced surface stresses, and thus the depth to the tip of the associated sheet – a topic of great importance during periods of volcanic unrest and when estimating the likelihood of sheet-fed eruption.

## Acknowledgements

We thank Weld on Sweden for financial support and Alessandro Tibaldi and an anonymous reviewer for helpful comments.

## References

Al Shehri, A., Gudmundsson, A., 2018. Modelling of surface stresses and fracturing during dyke emplacement: Application to the 2009 episode at Harrat Lunayyir, Saudi Arabia. J. Volcanol. Geotherm. Res., 356, 278-303.

Amadei, B., Stephansson, O., 1997. Rock Stress and its Measurement. Chapman and Hall, London.

Ancochea, E., Brandle, J.L., Huertas, M.J., Cubas, C.R., Hernan, F., 2003. The felsic dikes of La Gomera (Canary Islands): identification of cone sheet and radial dike swarms. J. Volcanol. Geotherm. Res., 120, 197-206.

Ancochea, E., Huertas, M.J., Hernan, F., Brandle, J.L., 2014. A new felsic cone-sheet swarm in the Central Atlantic Islands: the cone-sheet swarm of Boa Vista (Cape Verde). J. Volcanol. Geotherm. Res., 274, doi: 10.1016/j.volgeores.2014.01.010.

Anderson, E.M., 1936. The dynamics of formation of cone sheets, ring dykes and cauldron subsidences. Proc. Roy. Soc. Edinb.,, 56, 128-163.

Bagnardi, M., Amelung, F., Poland, M.P., 2013. A new model for the growth of basaltic shields based on deformation of Fernandina volcano, Galapagos Islands. Earth Planet Sci. Lett., 377-378, 358-366.
Barnett, Z.A., Gudmundsson, A., 2014. Numerical modelling of dykes deflected into sills to form a magma chamber. J. Volcanol. Geotherm. Res., 281, 1-11.
Bazargan, M., Gudmundsson, A., 2019. Dike-induced stresses and displacements in layered volcanic zones. J. Volcanol. Geotherm. Res., 384,189-205. .
Becerril, L., Galindo, I., Gudmundsson, A., Morales, J.M., 2013. Depth of origin of magma in eruptions. Scientific Reports 3, 2762. doi: 10.1038/srep02762
Bell, B.R., Claydon, R.V., Rogers, G., 1994. The petrology and geochemistry of cone-sheets from the Cuillin Igneous Complex, Isle of Skye: evidence for combined assimilation and fractional crystallisation during lithospheric extensions. J. Petrol., 35, 1055-1094.
Bistacchi, A., Tibaldi, A., Pasquarè, F..A., Rust, D., 2012. The association of cone–sheets and radial dykes: Data from the Isle of Skye (UK), numerical modelling, and implications for shallow magma chambers. Earth Planet. Sci. Lett., 339–340, 46-56.
Burchardt, S., Gudmundsson, A., 2009. Infrastructure of the Geitafell Volcano, Southeast Iceland. In: Thordarson, T., Self, S., Larsen, G., Rowland, S. K. Hoskuldsson (eds), A. Studies in Volcanology: The Legacy of George Walker. Special Publications of IAVCEI, 2, 349–369. The Geological Society of London, London.
Deb, D., 2006. Finite Element Method: Concepts and Applications in Geomechanics. Prentice-Hall, New Jersey.
Dering, G.M., Micklethwaite, S., Cruden, A.R., Barnes, S.J., Fiorentini, Marco L., 2019. Evidence for dyke-parallel shear during syn-intrusion fracturing. Earth Planet Sci. Lett., 507, 119-130.
Drymoni, K., Browning, J., Gudmundsson, A., 2020. Dyke-arrest scenarios in extensional regimes: Insights from field observations and numerical models, Santorini, Greece. J. Volcanol. Geotherm. Res., 396: doi.org/10.1016/j.jvolgeores.2020.106854
Dzurisin, D., 2006. Volcano Deformation. Springer Verlag, New York.
Foged, N.N., Andreassen, K.A., 2016. Strength and deformation properties of volcanic rocks in Iceland. In: Proc. 17$^{th}$ Nordic Geotechnical Meeting, pp. 1-10.
Galindo, I., Gudmundsson, A., 2012 Basaltic feeder-dykes in rift zones: geometry, emplacement, and effusion rates. Natural Hazards and Earth System Sciences, 12, 3683–3700.
Galland, O., Burchardt, S., Hallot, E., Mourgues, R., Bulois, C., 2014. Dynamics of dikes versus cone sheets in volcanic systems. J. Geophys. Res., 119, 6178-6192.
Gautneb, H., Gudmundsson, A., 1992. Effect of local and regional stress fields on sheet emplacement in West Iceland. J. Volcanol. Geoth. Res .51, 339-356.
Gautneb, H., Gudmundsson, A., Oskarsson, N., 1989. Structure, petrochemistry, and evolution of a sheet swarm in an Icelandic central volcano. Geol. Mag., 126, 659-673.
Geldmacher, J., Haase, K.M., Devey, C.W., Garbe-Schönberg, C.D., 1998. The petrogenesis of Tertiary cone-sheets in Ardnamurchan, NW Scotland: petrological and geochemical constraints on crustal contamination and partial melting. Contrib. Mineral. Petrol., 131, 196-209.

Gerbault, M., Cappa, F., Hassani, R., 2012. Elasto-plastic and hydromechanical models of failure around an infinitely long magma chamber. Geochem., Geophys., Geosyst., 13, doi: 1029/2011GC003917

Geshi, N., Kusumoto, S., Gudmundsson, A., 2010. Geometric difference between non-feeder and feeder dikes. Geology, 38, 195–198.

Geshi, N., Kusumoto, S., Gudmundsson, A., 2012. Effects of mechanical layering of host rocks on dike growth and arrest. J. Volcanol. Geotherm. Res., 223-224, 74-82.

Gudmundsson, A., 1995. Infrastructure and mechanics of volcanic systems in Iceland. J. Volcanol. Geotherm. Res., 64, 1-22.

Gudmundsson, A., 1998. Magma chambers modeled as cavities explain the formation of rift zone central volcanoes and their eruption and intrusion statistics. J. Geophys. Res., 103, 7401-7412.

Gudmundsson, A., 2003. Surface stresses associated with arrested dykes in rift zones: Bull. Volcanol., 65, 606-619.

Gudmundsson, A., 2011a. Rock Fractures in Geological Processes. Cambridge University Press, Cambridge.

Gudmundsson, A., 2011b. Deflection of dykes into sills at discontinuities and magma-chamber formation. Tectonophysics, 500, 50-64.

Gudmundsson, A., 2020. Volcanotectonics: Understanding the Structure, Deformation, and Dynamics of Volcanoes. Cambridge University Press, Cambridge.

Gudmundsson, A., Brenner, S.L., 2001. How hydrofractures become arrested. Terra Nova, 13, 456-462.

Gudmundsson, A., Loetveit, I.F., 2005. Dyke emplacement in layered and faulted rift zone. Journal of Volcanology and Geothermal Research, 144, 311-327.

Gudmundsson, A., Pasquare, F.A., Tibaldi, A., 2018. Dykes, sills, laccoliths, and inclined sheets in Iceland. In: Breitkreuz, C., Rocchi, S. (eds), Physical Geology of Shallow Magmatic Systems: Dykes, Sills and Laccoliths. Berlin, Springer, pp. 363-376.

Guldstrand, F., Burchardt, S., Hallot, E., Galland, O., 2017. Dynamics of surface deformation induced by dikes and cone sheets in cohesive Coulomb brittle crust. J. Geophys. Res., 122, 8511-8524.

Harker, A., 1904. The Tertiary Igneous Rocks of Skye. UK Geological Surv. Mem., 481 pp.

Heap, M.J., Villeneuve, M., Albino, F., Farquharson, J.I., Brothelande, E., Amelung, F., Got, J.L., Baud, P., 2020. Towards more realistic values of elastic moduli for volcano modelling. J. Volcanol. Geotherm. Res., 390, doi.org/10.1016/j.jvolgeores.2019.106684.

Klausen, M.B., 2004. Geometry and mode of emplacement of the Thverartindur cone sheet swarm, SE Iceland. J. Volcanol. Geotherm. Res., 138, 185-204.

Klausen, M.B., 2006. Geometry and mode of emplacement of dike swarms around the Birnudalstindur igneous centre, SE Iceland. J. Volcanol. Geotherm. Res .,151, 340-356.

Liu, G.R. , Quek, S.S., 2014. Finite Element Method, 2$^{nd}$ ed. Elsevier, Amsterdam.

Martí, J., C. López, S. Bartolini, L. Becerril, Geyer , A., 2016. Stress controls of monogenetic volcanism: a review. Front. Earth Sci., 4(106), doi: 10.3389/feart.2016.00106.

Martí, J., A. Villaseñor, A. Geyer, C. López, Tryggvason, A., 2017. Stress barriers controlling lateral migration of magma revealed by seismic tomography. Sci. Reports, 7, 40757, doi: 10.1038/srep40757

Meriaux, C., Lister, J.R., 2002. Calculation of dike trajectories from volcanic centers. J. Geophys. Res., 107, doi: 10.1029/2001JB000436

Morales Rivera, A.M., Amelung, F., Mothes, P., Hong, S.-H., Nocquet, J.-M., Jarrin, P., 2017. Ground deformation before the 2015 eruptions of Cotopaxi volcano detected by InSAR. Geophys. Res. Lett., 44, 6607-6615.

Okada, Y., 1985. Surface deformation due to shear and tensile faults in a half-space. Bulletin of the Seismological Society of America, 75, 1135-1154.

Okada, Y., 1992. Internal deformation due to shear and tensile faults in half space. Bulletin of the Seismological Society of America, 82, 1018-1040.

Pasquarè., F, Tibaldi., A., 2007. Structure of a sheet-laccolith system revealing the interplay between tectonic and magma stresses at Stardalur Volcano, Iceland. J. Volcanol. Geotherm. Res., 161, 131-150.

Philipp, S.L., Afsar, F., Gudmundsson, A., 2013. Effects of mechanical layering on hydrofracture emplacement and fluid transport in reservoirs. Frontiers in Earth Science, 1, doi:10.3389/feart.2013.00004

Phillips, W.J., 1974. The dynamic emplacement of cone sheets. Tectonophysics, 24, 69-84.

Rivalta, E., Taisne, B., Bunger, P., Katz, F., 2015. A review of mechanical models of dyke propagation: Schools of thought,results and future directions. Science Direct ,Tectono physics. 638, 1-42, doi.org/10.1016/j.tecto.2014.10.003.

Robinson, P.T., Mehegan, J., Gibson, I.L., Schmincke, H-U., 1982. Lithology and structure of the volcanic sequence in Eastern Iceland. J. Geophys. Res., 87, 6429-6436.

Schaefer, L.N., Kendrick, J. E., Oommen, T., Lavallee, Y., Chigna, G., 2015. Geomechanical rock properties of a basaltic volcano. Front. Earth Sci., 3: 29, doi: 10.3389/feart.2015.00029.

Schirnick, C., Bogaard, P. v.d., Schmincke, H-U., 1999. Cone sheet formation and intrusive growth of an oceanic island – the Miocene Tejeda complex on Gran Canaria (Canary Islands). Geology, 27, 207-210.

Scholz, C.H., 1990. The Mechanics of Earthquakes and Faulting. Cambridge, Cambridge University Press.

Segall, P., 2010. Earthquake and Volcano Deformation. Princeton University Press, Princeton.

Siler, D.L., Karson, J.A., 2009. Three-dimensional structure of inclined sheet swarms: Implications for crustal thickening and subsidence in the volcanic rift zones of Iceland. J. Volcanol. Geotherm. Res., 18, 333-346.

Stephens, T.L., Walker, R.J., Healey, D., Bubeck, A., England, R.W., 2018. Mechanical models to estimate paleostress state from igneous intrusions. Solid Earth, 9, 847-858.

Tibaldi., A, Pasquarè, F.A., Rust, D., 2011. New insights into the cone sheet structure of the Cuillin Complex, Isle of Skye, Scotland. J. Geol. Soc., 168, 689-704.

Tibaldi, A., Bonali, F., Pasquaré, F.A., Rust, D., Cavallo, A., D'Urso, A., 2013. Structure of regional dykes and local cone sheets in the Midhyrna-Lysuskard area, Snaefellsnes Peninsula (NW Iceland). Bull. Volcanol., 75: 764, doi 10.1007/s00445-013-0764-8.

Townsend, M.R., Pollard, D.D., Smith, R.P., 2017. Mechanical models for dikes: A third school of thought. Tectonophysics, 703-704, 98-118.

Troll, V.R., Carracedo, J.C., 2016. The Geology of the Canary Islands. Elsevier, Amsterdam.

Valko, P., Economides, M.J., 1995. Hydraulic Fracture Mechanics. Wiley, New York.

Walker, G.P.L., 1959. Geology of the Reydarfjordur area, eastern Iceland. Q.J. Geol. Soc. Lond., 114, 367-393.